Article

Cell Reports

Control of *Drosophila* Growth and Survival by the Lipid Droplet-Associated Protein CG9186/Sturkopf

Graphical Abstract

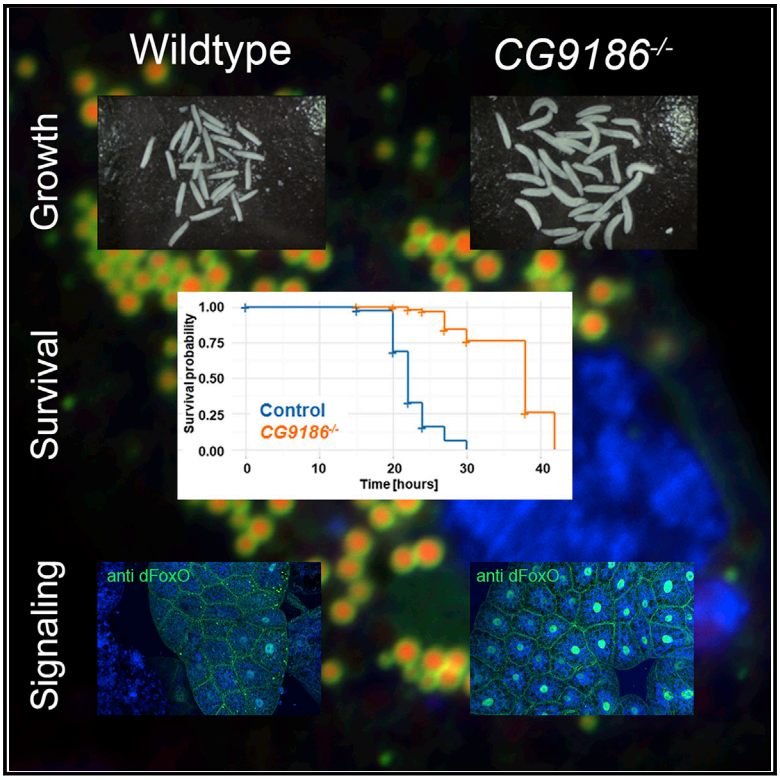

Authors

Michael Werthebach, Fiona A. Stewart, Alisa Gahlen, ..., Gereon Poschmann, Kai Stühler, Mathias Beller

Correspondence

mathias.beller@hhu.de

In Brief

Werthebach et al. introduce the lipid droplet-associated protein CG9186/sturkopf as a component of organismic physiology regulation, which affects insulin and juvenile hormone signaling activity.

Highlights

- CG9186/sturkopf mutants show a mild lipid storage phenotype
- The survival and response to dietary changes is altered in CG9186/sturkopf mutants
- CG9186/sturkopf function affects juvenile hormone and insulin signaling activities
- CG9186/sturkopf function links lipid droplets to organismic physiology regulation

Werthebach et al., 2019, Cell Reports *26*, 3726–3740
March 26, 2019
https://doi.org/10.1016/j.celrep.2019.02.110

CellPress

OPEN ACCESS
CellPress

Cell Reports
Article

Control of *Drosophila* Growth and Survival by the Lipid Droplet-Associated Protein CG9186/Sturkopf

Michael Werthebach,[1,2] Fiona A. Stewart,[1,2] Alisa Gahlen,[1,2] Tabea Mettler-Altmann,[3] Irfan Akhtar,[1,2] Kerstin Maas-Enriquez,[1,2] Andrea Droste,[1,2] Thomas O. Eichmann,[4] Gereon Poschmann,[5,6] Kai Stühler,[5,6] and Mathias Beller[1,2,7,*]

[1]Institute for Mathematical Modeling of Biological Systems, Heinrich Heine University Düsseldorf, 40225 Düsseldorf, Germany
[2]Systems Biology of Lipid Metabolism, Heinrich Heine University Düsseldorf, 40225 Düsseldorf, Germany
[3]Institute for Plant Biochemistry, Heinrich Heine University Düsseldorf, 40225 Düsseldorf, Germany
[4]Institute of Molecular Biosciences, University of Graz, 8010 Graz, Austria
[5]Molecular Proteomics Laboratory, Biomedical Research Center (BMFZ), Heinrich Heine University Düsseldorf, 40225 Düsseldorf, Germany
[6]Institute for Molecular Medicine, University Hospital Düsseldorf, Heinrich Heine University Düsseldorf, 40225 Düsseldorf, Germany
[7]Lead Contact
*Correspondence: mathias.beller@hhu.de
https://doi.org/10.1016/j.celrep.2019.02.110

SUMMARY

Lipid droplets (LDs) are the universal cellular storage organelles for esterified neutral lipids. The increasing number of characterized LD-associated proteins attained LDs with hitherto unexpected functions on top of their classical role as energy depot. Here, we characterize the LD-associated protein CG9186 of *Drosophila* by a CRISPR/Cas9-derived mutant fly line. While the mutant flies only showed a mild triacylglycerol storage phenotype, they were highly protected from desiccation stress, likely linked to a reduced locomotor activity and altered cuticular hydrocarbons. Both parameters depend on juvenile hormone (JH) signaling. Together with an observed interaction between CG9186 and JH-degrading enzymes, our results suggest that CG9186 participates in endocrine physiology regulation. In support of this hypothesis, CG9186 mutant flies show an altered expression of JH target genes and fail to adjust their developmental rate to dietary yeast-to-sugar ratio changes. Our results thus link LDs to organismic physiology regulation.

INTRODUCTION

Excess lipids, such as free fatty acids or cholesterol, are converted into neutral lipids such as triacylglycerols (TAGs) or cholesteryl esters (CEs) and stored in dedicated and omnipresent organelles called lipid droplets (LDs). From bacteria to humans, LDs share the same blueprint: a hydrophobic core with the storage lipids is surrounded by a phospholipid monolayer with proteins attached (Thiam and Beller, 2017). LDs mainly serve the regulated deposition and remobilization of energy-rich neutral lipids in times of nutrient excess and energy demand, respectively. More recently, however, LDs have also been associated with more diverse functions such as providing a platform for pathogen reproduction, playing a role as protein storage depots, or being involved in neurodegeneration (e.g., reviewed in Welte, 2015). Multiple signaling pathways converge on the surface of LDs, which thus represent an important cellular signaling platform (Arrese et al., 2014). Whether and how LDs additionally are directly involved in outbound signaling events is largely unknown. However, LDs affect organismic physiology profoundly. For example, they serve as a nutrient-sensing proxy in neuroendocrine cells affecting food intake behavior (Kaushik et al., 2011), and there is a tight correlation between LD deposits and different types of cancer, as for example in the prostate, where CE-enriched LDs promote cancer proliferation and growth, as well as tumor invasion capability (Yue et al., 2014). Furthermore, LDs are the source of building blocks for the synthesis of signaling molecules such as steroid hormones (Servetnick et al., 1995).

LD-associated proteins are key to their diverse functions. On top of a core set of a few dozen of LD-associated proteins (e.g., reviewed in Hodges and Wu, 2010), proteomic studies with LDs isolated from diverse cell lines, tissues, and organisms revealed the presence of likely hundreds of additional proteins (Beller et al., 2006; Cermelli et al., 2006; Ding et al., 2012; Fei et al., 2011; Li et al., 2016; Rösch et al., 2016; Schmidt et al., 2013; Vrablik et al., 2015; Zhang et al., 2011). While the role of selected LD-associated proteins, such as the perilipins, in energy metabolism regulation is well investigated (e.g., reviewed in Kimmel and Sztalryd, 2016), many proteins still lack a detailed analysis.

Here, we functionally characterize the evolutionarily conserved LD-associated protein CG9186 of *Drosophila melanogaster*. The protein localizes in the absence of LDs in the endoplasmic reticulum (ER) and targets LDs once they become available (Thiel et al., 2013). The detailed molecular function of CG9186 remains elusive. Due to the presence of a classical serine hydrolase catalytic triad, the protein was predicted to act as a lipase (Gramates et al., 2017; Thiel et al., 2013). Given that the protein is very abundant in the *Drosophila* fat storage tissue (Thiel et al., 2013) (the fat body), where LDs mostly contain

neutral lipids (e.g., TAGs) (Carvalho et al., 2012), an activity such as neutral lipid lipase (thus targeting TAG or diacylglycerol [DAG] or monoacylglycerol [MAG]) appeared likely. However, overexpression of the wild-type CG9186 protein, as well as its murine homolog lipid droplet-associated hydrolase (LDAH)/MGI:1916082, resulted in the induction of LD clusters in *Drosophila* or mammalian tissue culture cells and the salivary glands of *Drosophila* larvae (Thiel et al., 2013) instead of a remobilization of the LDs, as would have been expected for a lipolytic enzyme. The knock down of CG9186 in flies resulted in a mild decrease in TAG storage levels (Thiel et al., 2013). These findings, in combination with the negative results of direct enzymatic activity tests for TAG, DAG, and MAG hydrolyzing activity, strongly argued against a function as TAG lipase (Thiel et al., 2013). For mice, the data concerning the role of LDAH in TAG storage regulation is contradictory. One LDAH knockout mouse study did not show any TAG storage differences or other prominent lipid metabolism-associated phenotypes (Kory et al., 2017). Furthermore, the authors reported negative findings from different targeted lipid modifying enzyme activity assays (Kory et al., 2017). A second and independent LDAH knockout mouse study, however, revealed a significant weight gain by the mutant female mice as compared to their wild-type littermates (Currall et al., 2018). A third study demonstrated the role of LDAH in regulating the stability of the main TAG lipase adipose triglyceride lipase (ATGL) (Zimmermann et al., 2004) via polyubiquitination in HEK293 tissue culture cells (Goo et al., 2017). This study suggests that LDAH has a lipogenic function because the overexpression of LDAH enhanced the degradation of ATGL, and thus increased cellular TAG storage levels (Goo et al., 2017). These effects were independent of a hypothetical enzymatic activity of LDAH (Goo et al., 2017). While these findings argue against a prominent enzymatic function, the overexpression of a presumptive catalytically inactive form of CG9186, in which the predicted catalytically active serine was changed to an alanine, resulted in an enhancement of the LD clustering phenotype (Thiel et al., 2013). This finding may suggest a completely different enzymatic activity could be present or an activity that targets other lipid species. One study identified for the murine LDAH protein a CE hydrolase activity in macrophages (Goo et al., 2014), which are enriched for CE (Ouimet and Marcel, 2012), as are prostate cancer cells (Yue et al., 2014). However, neither of the aforementioned LDAH knockout studies found a corresponding CE storage phenotype in macrophages or other tissues (Currall et al., 2018; Kory et al., 2017). Given the unclear role of CG9186 and its relatives in TAG and CE metabolism, one could speculate that the proteins are operating outside the canonical lipid metabolism, perhaps affecting protein activity and/or stability, as demonstrated for ATGL (Goo et al., 2017). The identification of various prostate cancer risk-associated single-nucleotide polymorphisms (SNPs) in the human CG9186 orthologous gene, called c2orf43 (Du et al., 2016; Innocenti et al., 2011; Lindström et al., 2012; Long et al., 2012; Penney et al., 2015; Shui et al., 2014; Takata et al., 2010; Wang et al., 2013), suggests, for example, a role in signaling events affecting growth and proliferation control. Recently, a patient with a mutation in c2orf43 who suffers from prostate cancer and congenital hearing loss was identified and described (Currall et al., 2018). The study revealed a prominent role for the mouse and human CG9186-related proteins in prostate cancer initiation and progression via a very comprehensive and elegant set of experiments with various prostate cancer cell lines and an LDAH knockout mouse (Currall et al., 2018). Mechanistically, however, the connection between the loss of c2orf43/LDAH function and prostate cancer is not yet resolved. To investigate the *in vivo* function of CG9186 and potentially its mammalian homologs in greater detail, we generated a CG9186 loss-of-function fly mutant by CRISPR/Cas9 genome editing and present here its detailed functional characterization.

RESULTS

CG9186 Null Mutant Flies Store Less TAG

To investigate the function of CG9186 in an organismic context, we generated *Drosophila* flies carrying a genetic null mutation through the induction of a genomic deletion by CRISPR/Cas9 following the injection of two single-guide RNAs (sgRNAs) (for details, see Experimental Model and Subject Details and Figure S1). The CRISPR/Cas9-induced double-strand breaks were designed to result in a deletion spanning approximately 1.1 kbp, covering a part of the 5′ UTR and most of the CG9186 coding sequence (Figures 1A and S1). Western blot analysis with a CG9186-specific antiserum (Thiel et al., 2013) revealed a lack of CG9186 protein signal in the homozygous state of different alleles generated (Figures 1B and S1B). The CG9186 mutant flies were viable and showed no gross fertility defects under standard nutritional conditions (Figure S1C). In line with our previous experiments, which demonstrated a TAG reduction phenotype following ubiquitous RNAi-mediated CG9186 depletion (Thiel et al., 2013), 6-day-old virgin female and male CG9186 loss-of-function individuals showed significantly reduced TAG storage levels when compared to a genetically matched control fly strain (Figure 1C). Because all of the CG9186 mutant strains were phenotypically virtually indistinguishable, all of the following experiments are shown for the *CG9186[35.7]* allele.

We tested next whether the CG9186 loss-of-function mutation also causes a TAG storage phenotype before the animals reach the adult stage. However, neither embryos laid by homozygous mutant mothers nor whole third-instar mutant larvae showed altered TAG storage levels (Figures S1D and S1E). Given the large amount of CG9186 protein in LDs purified from larval fat body preparations (Beller et al., 2006; Thiel et al., 2013), we took a closer look at the fat body LDs. However, we detected neither any morphological differences (Figure S1F) nor a prominent effect on the lipid composition of purified third-instar larval fat body LDs following lipidomics analysis (Figure S1G).

To investigate the TAG storage phenotype of the adult CG9186 mutant flies further, we asked next whether key parameters influencing lipid storage amounts are affected, which potentially explain the reduced lipid storage phenotype. A food intake quantification of the control and *CG9186[35.7]* mutant flies using fluorescein-containing food did not reveal any differences (Figure S2A). Flies kept at 4°C, which blocks food consumption, or starvation of the flies before the food intake experiment, which enhances food intake, served as positive

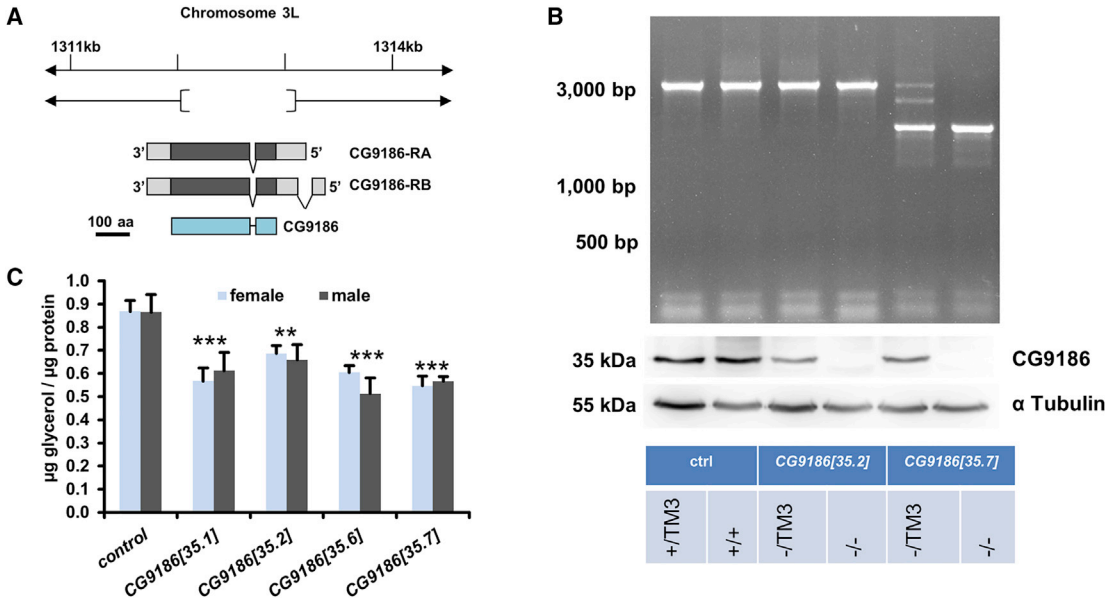

Figure 1. Generation of a CG9186 Null Mutation Fly and Its Triacylglycerol Storage Phenotype

(A) Genomic locus of the CG9186 gene and targeted deletion area. mRNA is shown below for the two annotated transcript isoforms. Light gray represents untranslated region and dark gray represents coding sequence. The resulting polypeptide is shown in blue.

(B) PCR- (top) and western blot (bottom)-based characterization of heterozygous and homozygous CG9186 loss-of-function fly lines, as well as the genetically matched control. The 35.2 allele carries an indel mutation resulting in a premature stop codon. Data for additional mutant lines, sequence information of the deletion and the oligonucleotide, and guide RNA sequences can be found in Figure S1.

(C) Triacylglycerol (TAG) storage levels of *ad libitum*-fed 7-day-old female and male CG9186 loss-of-function fly lines and a genetically matched control line. Light blue represents female flies and gray bars represent male flies. The statistical significance of differences between the male or female control (ctrl) and the respective corresponding CG9186 mutant flies were determined with a one-way ANOVA and a Tukey post hoc test.

Significance levels: n.s., $p \geq 0.05$, *$p < 0.05$, **$p < 0.01$, and ***$p < 0.001$. The bars in (C) represent the mean values of at least triplicate measurements. Error bars represent SDs.

controls. Next, we tested whether an increased locomotor activity could explain the lowered TAG storage levels and found that the averaged and total activities between control and CG9186 mutant flies did not differ significantly (Figure S2B). To investigate whether the CG9186 mutant flies stayed leaner due to a reduced lipogenesis capability, we provided 7-day-old male CG9186 and control flies with a high-fat diet containing 10% coconut oil. While CG9186 flies are capable of increasing their TAG storage amounts (Figure S2C), they always stayed leaner than the control flies. These results suggest that the lipogenesis capacity does not limit the CG9186 mutant TAG storage levels. Finally, we tested whether the 7-day-old CG9186 mutant flies had problems in remobilizing and restoring their lipid reserves. For this purpose, we subjected the flies to a starvation and refeeding paradigm (Figure S2D). CG9186 mutant flies are able to both mobilize the stored lipids and refuel them, however.

Based on the previously reported CE hydrolase activity of the murine CG9186 homolog LDAH (Goo et al., 2014), we also tested whether the CG9186 null mutant shows changes in the CE storage levels. The mutation of a CE mobilizing enzyme should result in increased CE storage levels. However, the CG9186 loss-of-function animals showed no difference in cholesterol and CE levels during the larval stage (Figure S2E) and only slightly reduced levels during the adult stage (Figure S2F). We investigated next whether the reduced TAG storage phenotype of adult CG9186 mutant flies could be indicative of a stress-response or general fitness defect.

The Mutation of CG9186 Affects Survival

Based on the reduced TAG storage amounts, we expected that 6-day-old CG9186 mutant flies would be sensitive toward starvation stress, which we confirmed (Figure S3A; $p < 0.0001$, log-rank test). Lowered TAG storage levels may be indicative of a dietary restriction, which extends lifespan (Finkel, 2015). The overall lifespan of the lean CG9186 mutant flies, however, was not prominently affected (Figure S3B), and yet we detected a stochastic premature male-specific lethality (Figure S3B). This finding could count as another indication of a general fitness defect. Therefore, we treated the flies with the insecticide paraquat, which induces oxidative stress and lethality (Rzezniczak et al., 2011), given that animals with a reduced overall fitness may be generally more sensitive to stress conditions. Both female and male 7-day-old mated CG9186 mutant individuals showed a reduced lifespan as compared to the control animals ($p < 0.0001$, log-rank test; Figure S3C). The basal oxidative stress levels, as detected by the measurement of thiobarbituric acid reactive substances (TBA-RS), however, were not significantly different between mutant and control animals in both sexes (Figure S3D). In conclusion, our findings thus far were

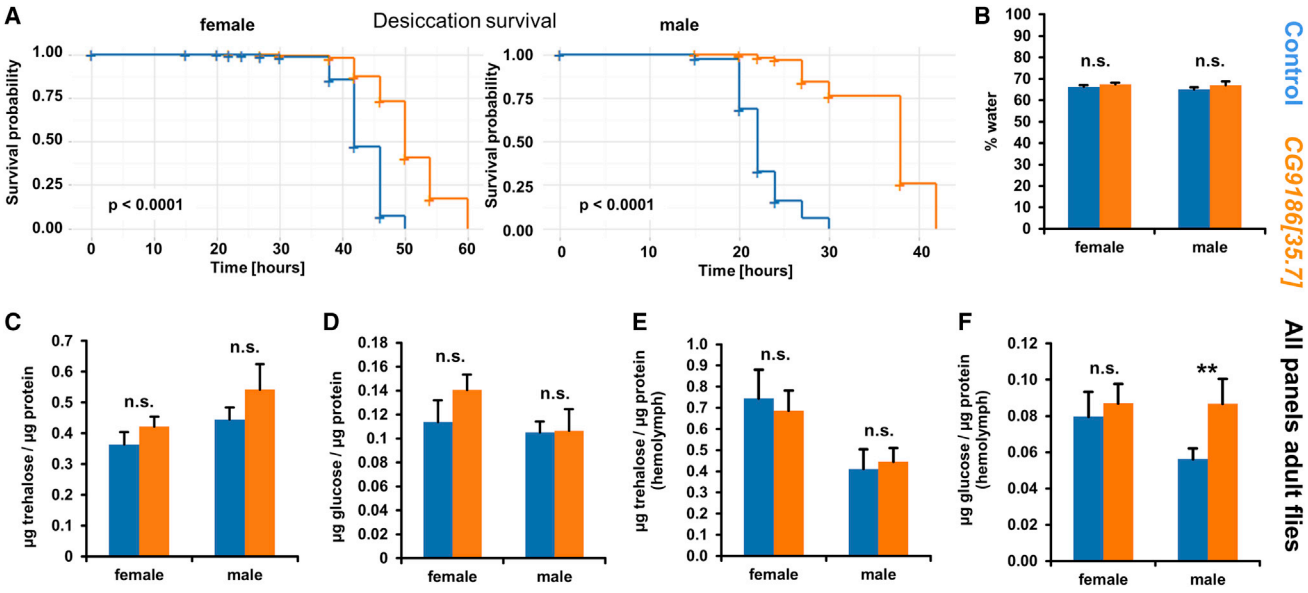

Figure 2. CG9186 Mutant Animals Are Protected from Desiccation Stress

(A) Seven-day-old control or CG9186 mutant flies were subjected to a desiccation experiment. The mutant animals are protected from the desiccation.

(B) The water content of 7-day-old reference and CG9186 loss-of-function female and male flies does not differ.

(C–F) Whole-body trehalose (C) and glucose (D) and hemolymph trehalose (E) levels are unaffected by the CG9186 loss-of-function mutation. Hemolymph glucose levels are elevated in the CG9186 mutant male individuals (F).

Blue indicates the genetically matched control, orange represents the CG9186 loss-of-function mutant. Bars in (B)–(F) represent mean values of at least triplicate measurements. Error bars represent SDs. Statistical significance for the Kaplan-Meier plots in (A) was estimated by a log-rank test; statistical significance in (B)–(F) was estimated by independent two-sample t tests. Significance levels: n.s., $p \geq 0.05$, *$p < 0.05$, **$p < 0.01$, and ***$p < 0.001$.

compatible with a general fitness defect of the CG9186 mutant flies; yet, when we analyzed the response of the mutant to desiccation stress, this view completely changed.

CG9186 Mutant Flies Are Protected from Desiccation

Elevated TAG storage levels tightly correlate with an increased desiccation resistance (Djawdan et al., 1998; Gefen et al., 2006; Parkash and Aggarwal, 2012; Yoshida et al., 2016). Thus, our expectation was that the decreased TAG storage levels of the CG9186 mutant in combination with its potential fitness defect result in a decreased desiccation resistance. However, the CG9186 mutant animals significantly outlived the control flies, with median survival times of 50 versus 42 h (females) or 38 versus 22 h (males) for the mutant and control flies, respectively (Figure 2A; for both sexes $p < 0.0001$, log-rank test). This prominent protection from desiccation stress strongly argued against a general fitness defect.

CG9186 Mutants Show a Decreased Locomotor Activity and Altered Cuticular Hydrocarbons

To investigate the basis for the desiccation resistance, we examined parameters known to alter the desiccation response. Here, aside from the hemolymph trehalose and glucose levels and the overall water content (Djawdan et al., 1998; Gefen et al., 2006; Parkash and Aggarwal, 2012; Yoshida et al., 2016), the locomotor activity and the cuticular hydrocarbon (CHC) levels and composition play an important role (Arcaz et al., 2016; Chung and Carroll, 2015; Dembeck et al., 2015).

The overall water content did not differ between the control and mutant flies (Figure 2B). We also did not find significant differences in the whole-body trehalose and glucose levels (Figures 2C and 2D), or the amount of trehalose in the hemolymph (Figure 2E), between the control and CG9186 mutant animals. However, the hemolymph glucose levels of CG9186 mutant male flies were consistently significantly increased (Figure 2F). The locomotor activity of CG9186 mutant flies kept without water was significantly lower as compared to that of the control animals (Figures 3A and 3B). We found this interesting because under basal conditions, we did not detect differences in the locomotor activity of CG9186 mutant and control animals (Figure S2B). We investigated next the CHC composition. For this purpose, we rinsed control and CG9186 mutant female and male flies in hexane and analyzed the CHC composition by gas chromatography coupled to tandem mass spectrometry. The CHC elution profile of female and male flies (Figure 3C) revealed clear-cut sex-specific differences in which female CHCs tend to elute at later retention times and therefore tend to have longer chain lengths, which is consistent with previous reports (Dembeck et al., 2015). Among the control and mutant animals, we identified several peaks with an altered abundance. The male samples showed more peak differences as well as higher overall abundance changes (Table S2). Given that higher CHC levels correlate with increased desiccation resistance, we focused on the peak eluting after 24.05 min (Figures 3C, 3D, and S4A), which showed on average a 5.8-fold increase in the CG9186 mutant as compared to the control animals. Fragmentation of the

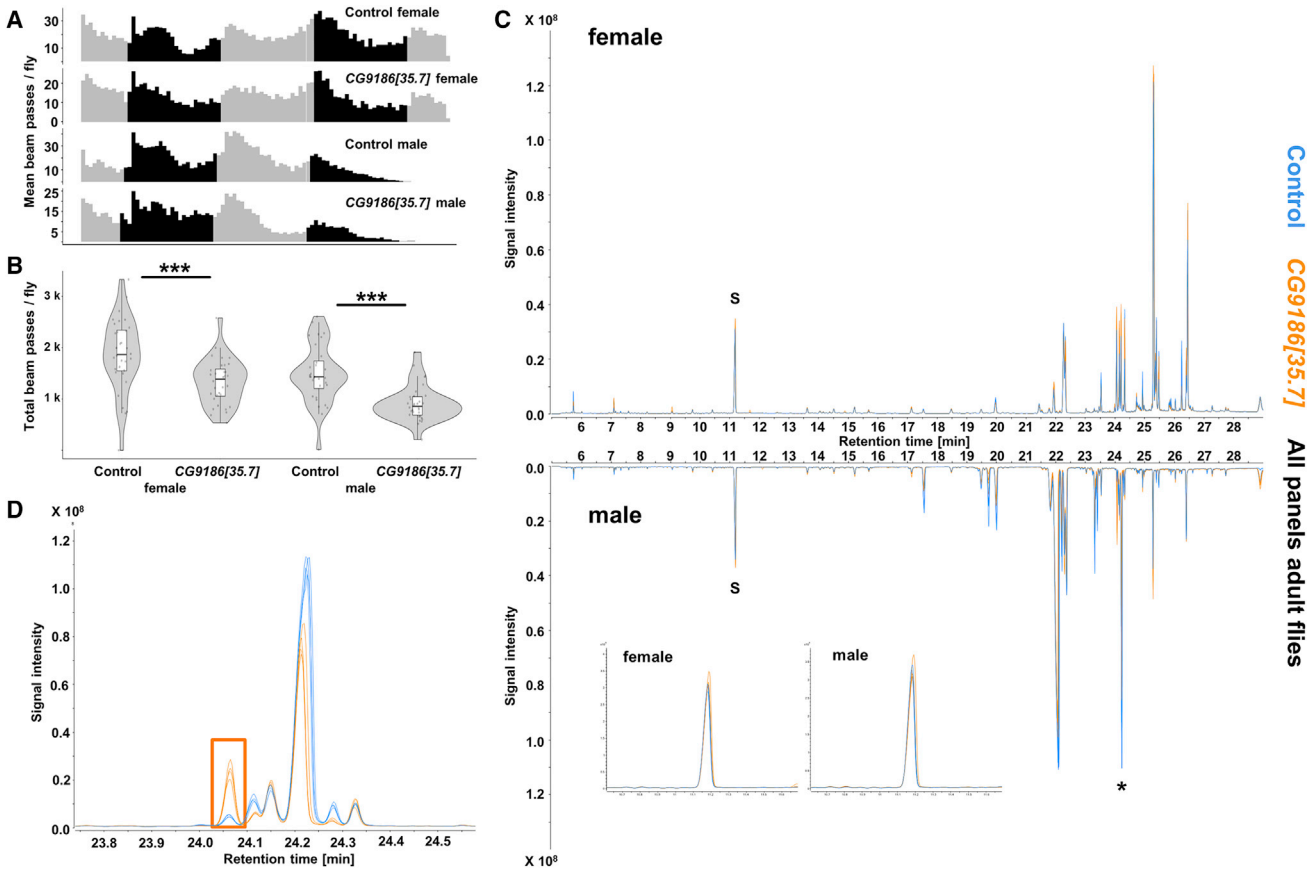

Figure 3. The Mutation of CG9186 Affects the Locomotor Activity during Desiccation and the Cuticular Hydrocarbon Composition

(A) Locomotor activity of 7-day-old control or CG9186 mutant female and male flies during desiccation. Phases with light (12 h/d) are represented by gray shading. Dark phases (12 h/d) are represented by black shading.

(B) Total activity counts per fly for the actinograms shown in (A). Per condition, 32 flies were monitored.

(C) Gas chromatography-mass spectrometry (GC-MS) analysis of the CHC composition of 14-day-old female (top) or male (bottom) control or CG9186 mutant flies. Blue corresponds to the control and orange to the CG9186 mutant animals. For the quantification of the CHC levels, we included a spike-in control during the extraction procedure (octadecane; S). The spike-in levels were highly similar across all of the samples (insets in the male spectrum graph).

(D) Close-up representation of the asterisk-highlighted peak group from (C). Detailed quantification and peak identification results are shown in Figure S4.

Significance levels in (B) were determined by independent two-sample t tests: n.s., $p \geq 0.05$ and ***$p < 0.001$.

associated compound and database search of the corresponding spectrum identified the compound as 2-methyltetracosane (2-ME; $C_{25}H_{52}$; Figures S4B and S4C). 2-ME is a known component of the *Drosophila* CHC repertoire (Everaerts et al., 2010), and its abundance changes with temperature shifts (Bontonou et al., 2013). Together with the reduced locomotor activity, the altered CHC abundance likely contributes to the desiccation resistance phenotype.

The CG9186 Protein Interacts with Juvenile-Hormone-Degrading Enzymes

We asked next how CG9186 could alter the locomotor activity upon desiccation stress as well as the CHC composition. Given that the juvenile hormone (JH) signaling pathway regulates both the composition and abundance of CHCs of diverse arthropods (Kelstrup et al., 2014, 2017; Lengyel et al., 2007) and was linked to the regulation of foraging behavior and locomotor activity (Meunier et al., 2007), the previously detected interaction between CG9186 and JH epoxide hydrolase (JHEH) enzymes (Kolkhof et al., 2017), which degrade JH in different tissues (Lü et al., 2015; Tusun et al., 2017; Wojtasek and Prestwich, 1996), was of particular interest. The JHEH enzymes complement the activity of the secreted JH esterase, which degrades JH in the hemolymph (Kamimura et al., 2007; Kamita and Hammock, 2010; Vermunt et al., 1997). Little is known concerning the regulation of JHEH enzymes. Here, we speculated that the interaction with CG9186 could interfere with JHEH function, and thus JH signaling activity.

The *Drosophila* genome encodes three JHEH enzymes (Gramates et al., 2017). We previously found an interaction between CG9186 and the JHEH1 enzyme in co-immunoprecipitation experiments (Kolkhof et al., 2017). An independent large-scale yeast-2-hybrid screen additionally revealed an interaction between CG9186 and JHEH3 (Guruharsha et al., 2011). To

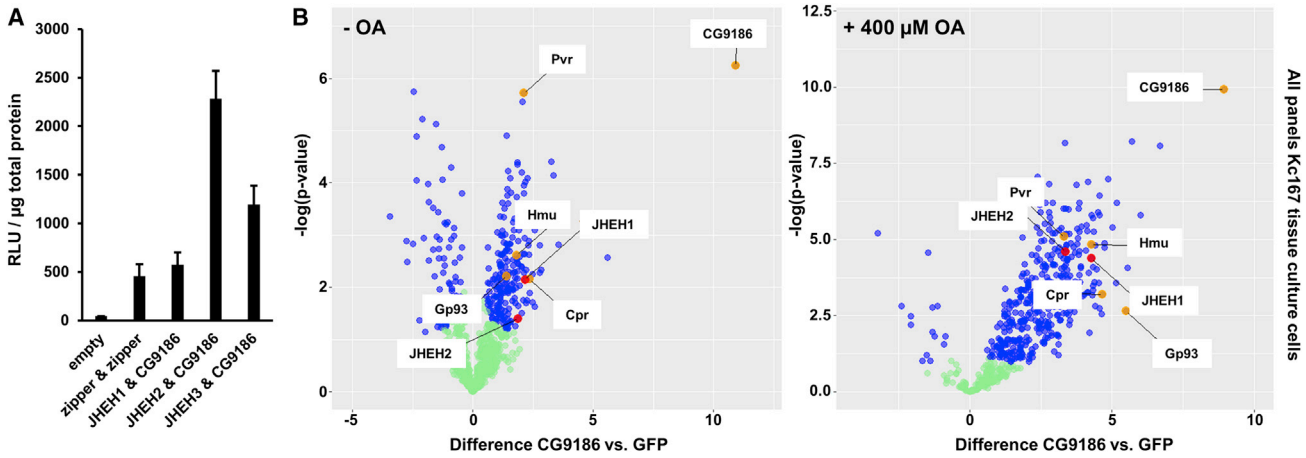

Figure 4. CG9186 Interacts with Juvenile-Hormone-Degrading Enzymes

(A) Split luciferase complementation protein-protein interaction assays between CG9186 and JHEH1, JHEH2, and JHEH3. The interaction of the GCN4 leucine zipper served as a positive control, as previously described (Kolkhof et al., 2017). Untransfected cells ("empty") served as a negative control. Bars represent mean values of triplicate measurements. Error bars represent SD.

(B) Volcano plots showing the enrichment of CG9186 interaction partners identified in co-immunoprecipitation experiments performed with cell lines expressing either GFP alone or a CG9186:GFP fusion protein in the absence (left; -OA) or the presence of 400 µM oleic acid (right; + 400 µM OA). For details, see main text and Figure S5.

Statistical significance (significant differential abundant proteins were determined using the significance analysis of microarrays method with a cutoff at a false discovery rate of 5%) is indicated in blue. Enrichment of CG9186 and the previously described CG9186 interaction partners (Kolkhof et al., 2017) Pvr, Hmu, Gp93, and Cpr is shown by labeling the corresponding points in orange. Red dots mark the juvenile hormone epoxide hydrolases (JHEHs) 1 and 2, which have been identified as putative CG9186 interaction partners. All proteomics data are provided in Table S2.

validate the CG9186 and JHEH enzyme interactions, we used a split-luciferase complementation assay system in which putative interactors are fused with fragments of the *Gaussia princeps* luciferase enzyme (Kolkhof et al., 2017). If the two proteins interact, then the luciferase enzyme activity is restored and is easily detectable in a plate-reader-compatible assay format. The baseline luciferase activity was measured with untransfected cells ("empty"), and the GCN4 leucine zipper interaction ("zipper & zipper") served as a positive control, as previously reported (Kolkhof et al., 2017). Luciferase activity levels above the positive control interaction were considered successful complementations, and thus interactions. In this assay, all three JHEH enzymes showed an interaction with CG9186 (Figure 4A). Additional co-immunoprecipitation experiments performed in the presence or absence of oleic acid-induced LDs (Figure S5; Table S2) confirmed the previously detected (Kolkhof et al., 2017) CG9186 interactions with hemomucin, cytochrome-P450 reductase (Cpr), the glycoprotein of 93 kDa (Gp93), or the platelet-derived growth factor (PDGF)- and vascular endothelial growth factor (VEGF)-receptor related (Pvr) proteins (Figure 4B). The experiments further confirmed the interactions between JHEH1 or JHEH2 and CG9186 (Figure 4B), yet we failed to detect an interaction with JHEH3. According to FlyBase (Gramates et al., 2017), however, JHEH3 expression is lowest in the Kc167 cells used for the co-immunoprecipitation (co-IP) experiments, thus potentially explaining the lack of identification. Based on these results, we developed the hypothesis that the interaction between CG9186 and the JHEH enzymes could alter JHEH activity and thus serve a regulatory function.

CG9186 Is Required to Adjust the Developmental Timing to Varying Nutritional Yeast-to-Sugar Ratios

To investigate the putative role of CG9186 in JH signaling and physiology regulation further, we changed again to the larval stage. Here, JH together with ecdysone signaling is required for the appropriate timing of the larval moltings and pupariation (Kayukawa et al., 2017; Mitsui and Riddiford, 1978). Recent results additionally demonstrated the impact of JH signaling on the rate of development, which is mediated by altered insulin/insulin-like growth factor (IIS) signaling and ultimately the *Drosophila* Forkhead box sub-group O (dFoxO) transcription factor activities (Mirth and Shingleton, 2012; Mirth et al., 2014). To challenge the developmental timing of the larvae, we altered the sugar-to-yeast content of the food, as low yeast content decelerates and low sugar content accelerates the rate of development. To quantify the diet-induced effects on the developmental timing, we measured the size of the developing larvae and recorded the time necessary to reach pupariation. On the control diets, the size of the 5-day-old larvae did not differ significantly between CG9186 mutant and control animals (Figures 5A and 5B). On the low-sugar diet, in contrast, the control animals reached after 5 days a significantly larger size as compared to the CG9186 mutant larvae (Figures 5A and 5B). The low-yeast diet caused both genotypes' prominent developmental retardation. The CG9186 mutant larvae, however, were much less severely affected as compared to the control animals (Figures 5A and 5B). Five days after egg laying, the CG9186 mutant larvae were on average ~58% larger compared to the control animals. After 9 days, size differences between the CG9186 mutant and control animals stayed about

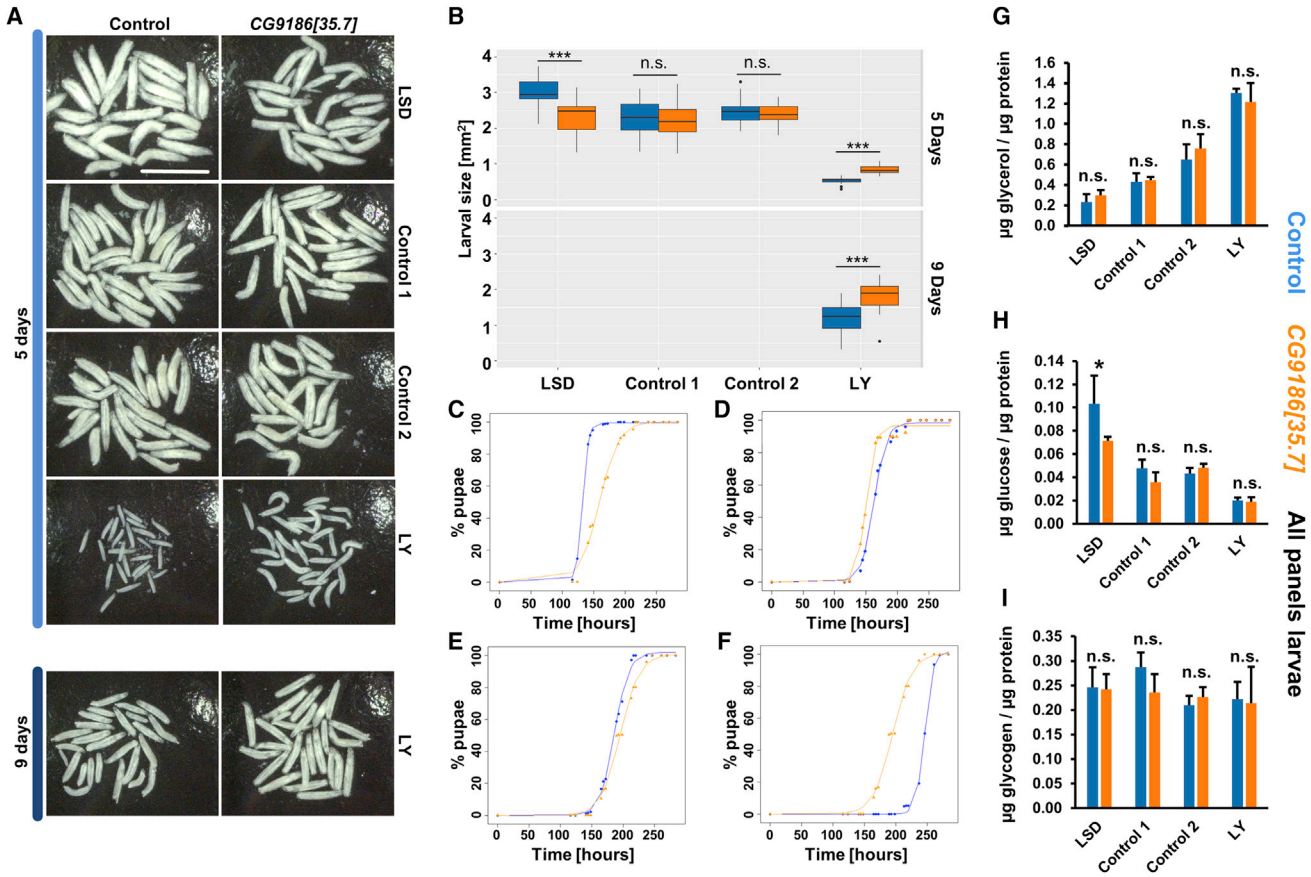

Figure 5. CG9186 Affects the Larval Growth Rate

(A) Micrographs of control or CG9186 mutant larvae raised on a low-sugar diet (LSD), two control diets (control 1 and 2), or a low-yeast diet (LY) (5 or 9 days after egg laying).

(B) Larval sizes from (A) were quantified from the microscopic images, and the results for the different diets are visualized using boxplots.

(C–I) The time to pupariation was also measured for animals reared on LSD (C), control diet 1 (D), control diet 2 (E) and LY (F). The TAG (G), glucose (H), and glycogen (I) levels for wandering third-instar larvae reared on the different diets were measured and normalized to total protein content.

Blue represents the genetically matched control and orange represents the CG9186 loss-of-function mutant. Boxplots in (B) are based on measurements of at least 19 larvae. Bars in (G)–(I) represent mean values of at least triplicate measurements. Error bars represent SDs. In (B) and G)–(I), independent two-sample t tests were used to test for statistical significance. Significance levels: n.s., $p \geq 0.05$, *$p < 0.05$, **$p < 0.01$, and ***$p < 0.001$. The scale bar in (A) represents 5 mm.

the same, with CG9186 larvae being ~49% larger than the controls (Figures 5A and 5B).

The size measurements correlated with the quantification of the time needed to reach pupariation. Under basal nutritional conditions, we noted only modest growth differences (50% pupae on control food 1 after 163 [control] versus 150 [mutant] h; on control food 2 after 185 [control] versus 195 [mutant] h, respectively; Figures 5D and 5E). Under low-sugar diet conditions, the development of the CG9186 mutant was slowed down significantly (50% pupae after 133 [control] versus 159 h [mutant], respectively; Figure 5C). Under low-yeast diet conditions, the CG9186 mutant developed more quickly (50% pupae after 246 [control] versus 195 [mutant] h, respectively) (Figure 5F; false discovery rate (FDR) corrected p value for all growth curve comparisons: $p < 0.05$). The CG9186 mutant larvae thus showed a much less prominent response to varying nutritional conditions. For the wild-type animals, the time span needed to reach 50% pupariation varied by 113 h (from 133 to 246 h after egg laying for the low-sugar and low-yeast diets, respectively). For the CG9186 mutant, however, the time span variation was with 45 h much lower (from 150 to 195 h after egg laying for the control food 1 and low-yeast diets, respectively). Since the CG9186 mutant larvae did not adjust their developmental timing to the nutritional conditions, it prompted us to name CG9186 "sturkopf" ("sturkopf" is the German translation for "stubborn person").

As a control, we tested whether the number of eggs laid and survival of the control or mutant animals on the different diets differed prominently; they did not (Figure S6). In addition, we tested whether the various nutritional conditions would affect the storage nutrient amounts of the control and mutant animals differently. For this purpose, we collected larvae close to pupariation and measured the TAG, glucose, and glycogen levels of the animals (Figures 5G–5I). Under basal nutritional conditions, the reference and mutant larvae had similar TAG storage amounts, as expected (Figure S1E), and the glucose and glycogen levels did not differ. Growth on the low-sugar diet

resulted in lower TAG storage amounts but increased glucose levels, whereas glycogen amounts remained unaffected. The CG9186/sturkopf mutant larvae showed slightly lower glucose levels as compared to the control animals (Figure 5H). When the animals developed on the low-yeast diet, TAG storage levels were increased in both genotypes, whereas glucose levels were diminished when compared to the growth under standard conditions. The storage nutrient amounts did not differ prominently between the CG9186/sturkopf mutant and control animals despite the variation of the yeast-to-sugar content in the food. Thus, metabolic differences are unlikely to contribute to the observed developmental timing phenotype.

CG9186/Sturkopf Triggers Expression of Nutritionally Regulated Transcripts

We tested next whether the altered developmental timing during the larval stage correlates with transcript-level changes in genes involved in nutritional sensing and growth control. Because IIS signaling is known to affect the rate of development, in part in cooperation with JH signaling (Mirth et al., 2014), we quantified the expression of different *Drosophila insulin-like peptides* (*dilps*) and their downstream target *d4E-BP* (*thor*). As a proxy for JH-signaling activity, we quantified the expression of the early JH target gene *Kruppel homolog 1* (*Kr-h1*) (Kayukawa et al., 2012). IIS acts in concert with the glucagon ortholog adipokinetic hormone (Akh) signaling pathway, which in turn regulates, for example, *dilp3* gene expression in larvae (Kim and Neufeld, 2015). Finally, IIS and Akh control the prominent gene expression changes of the target of brain insulin (*tobi*) gene in response to changes in the sugar-to-yeast ratio of the food (Buch et al., 2008).

For a significant gene expression change, we set the arbitrary threshold to at least 1.5-fold upregulation or 0.5-fold downregulation as compared to the expression in the wild-type control and $p < 0.05$ based on a permutation test (for details, see Experimental Model and Subject Details). CG9186 expression itself was not changed by the altered nutritional conditions (data not shown). We first compared how the mutation of CG9186/sturkopf affected the gene expression under basal conditions (Figure 6A). Based on the above-mentioned criteria, we found a significant downregulation of *dilp6* and a highly significant downregulation of *tobi* under the basal nutritional conditions (Figure 6A). In addition, on the low-yeast (Figure 6B) and low-sugar diets (Figure 6C), *tobi* expression was nearly absent. While on the low-yeast diet, no other gene was transcriptionally significantly altered; on the low-sugar diet, *dilp3*, *dilp6*, *Kr-h1*, and *thor* expression was significantly decreased as compared to the control (Figure 6C). *tobi* expression, however, was the most severely affected in all conditions.

We tested next whether the previously shown gene expression change of *tobi* following alterations of the sugar-to-yeast ratio of the food was altered by the CG9186/sturkopf mutation. As previously reported (Buch et al., 2008), growth on a low-yeast diet significantly reduced *tobi* expression, whereas *tobi* was highly upregulated following growth on a low-sugar diet (Figure 6D). In CG9186/sturkopf mutants, this regulation was completely absent, and gene expression levels were not altered by growth on the different diets (Figure 6D). This finding further consolidates the limited response of CG9186/sturkopf mutants to varying nutritional cues. *Kr-h1* expression was decreased on the low-yeast diet in the control and CG9186/sturkopf flies to a similar level (Figure 6E). When the animals were raised on the low-sugar diet, however, *Kr-h1* was upregulated in the control animals, but not in the CG9186/sturkopf mutant flies (Figure 6E). This finding supports a JH degradation limiting function of CG9186, which prohibits the upregulation of JH activity, whereas a decrease in JH activity is still possible.

To test whether CG9186/sturkopf is also sufficient to alter gene expression, we used the Gal4/upstream activating sequence (UAS) system to overexpress a GFP-tagged CG9186 variant (Thiel et al., 2013). On top of the ubiquitous overexpression, we used fat body- and oenocyte-specific activator lines. We chose those tissues based on the strong expression of CG9186 in the fat body (Beller et al., 2006; Thiel et al., 2013) and the desiccation and CHC phenotype of CG9186, which is indicative of an oenocyte function. On top of *tobi* and *Kr-h1* expression, we monitored expression of *dilp3*, *dilp6*, and *thor,* as those were differently expressed in the CG9186/sturkopf mutant (Figure 6A). Ubiquitous activation of the CG9186:GFP transgene resulted in the strongest overexpression (Figure 6F). The fat body-derived expression levels were only moderately lower and oenocyte-specific activation was still detectable, despite the very local activity of the Gal4 activator (Figure 6F). *dilp3*, *dilp6*, and *thor* did not show prominent gene expression changes following the ubiquitous or fat body-specific overexpression of CG9186/sturkopf (Figure S7). The oenocyte-specific expression of CG9186/sturkopf caused a marginal upregulation of *dilp3* and *dilp6* expression levels. For *Kr-h1*, ubiquitous and oenocyte-specific overexpression of CG9186:GFP resulted in increased expression levels. Oenocyte-specific overexpression further resulted in increased *tobi* expression levels (Figure 6F). The fat body-specific activation, in contrast, did not result in prominent *tobi* and *Kr-h1* gene expression changes, despite its much higher magnitude of CG9186/sturkopf transcript abundance as compared to the oenocyte expression.

Nuclear dFoxO Is Increased in CG9186/Sturkopf Mutant Larvae

dFoxO is a central player in organismic physiology regulation (DiAngelo and Birnbaum, 2009; Kousteni, 2012). Its activity is important for several of the phenotypes observed by us as it represses, for example, *tobi* expression (Buch et al., 2008); is a proxy for IIS activity (Giannakou et al., 2004), which is reduced in the CG9186/sturkopf mutant; and is important for altering the rate of development downstream of JH perturbation (Mirth et al., 2014). dFoxO is a transcription factor, which is expelled from the nucleus by phosphorylation downstream of IIS activation. To directly test whether dFoxO activity is altered in CG9186/sturkopf mutant animals, we stained wandering third-instar larval fat bodies with a specific dFoxO antibody and monitored its subcellular localization (Figure 7A). In control animals kept on a standard diet, dFoxO was occasionally nuclear; however, most nuclei lacked a clear-cut signal (Figure 7A), which is comparable to previous reports (Buch et al., 2008). In CG9186/sturkopf mutant animals, however, many nuclei showed a very strong signal (Figures 7A and 7B), indicative of decreased IIS

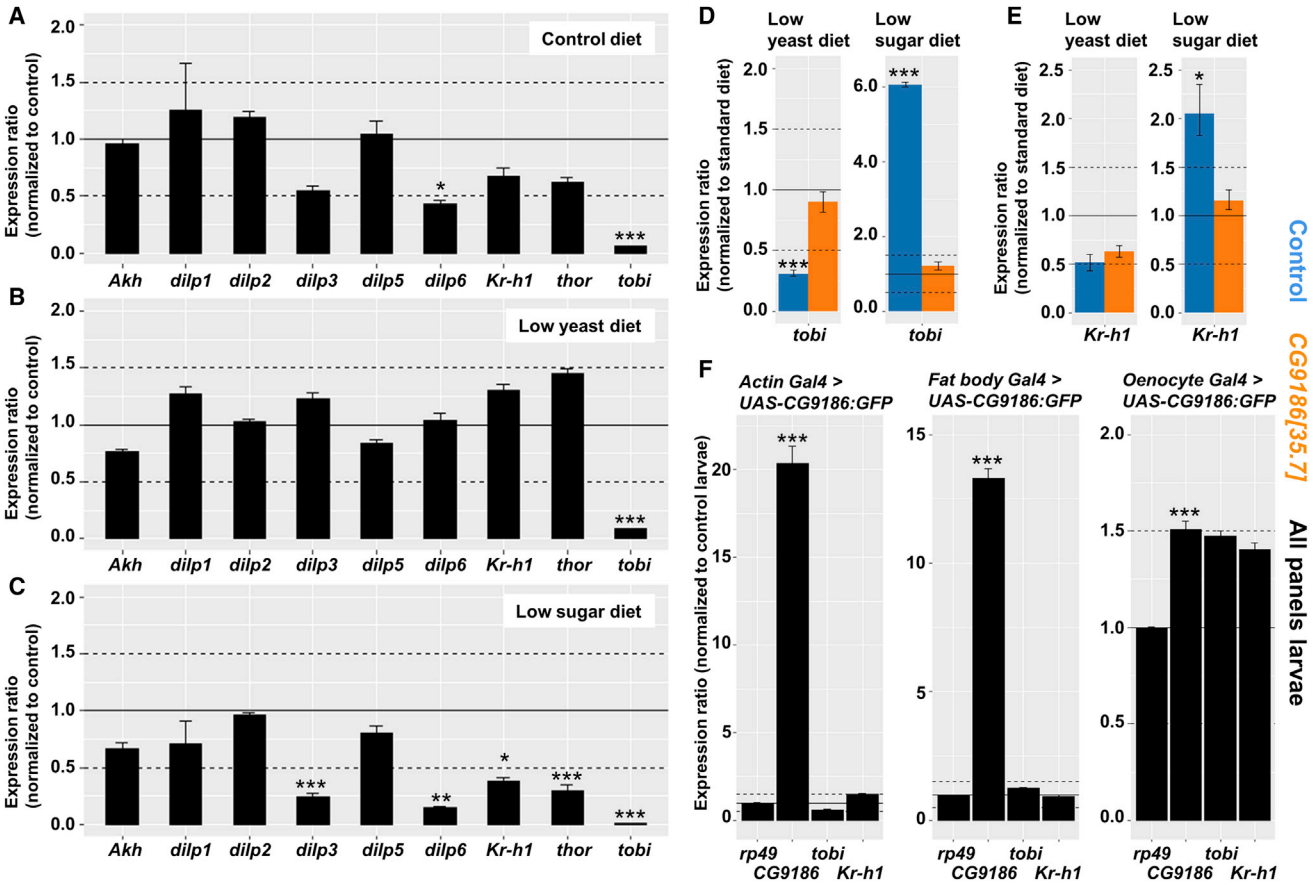

Figure 6. CG9186 Affects the Transcriptional Response to Altered Nutrient Conditions

(A) qPCR-based gene expression analysis of 5-day-old control or CG9186 mutant larvae raised on a standard diet. Expression was normalized to the *rp49* expression and the genetically matched control of the CG9186 mutant.

(B–E) The same experiment in (B) as in (A), but with larvae reared on a low-yeast or (C) low-sugar diet. Gene expression change of the *tobi* (D) or *Kr-h1* (E) gene for the low-yeast (left plot) or low-sugar (right plot) diet for the control and CG9186 mutant larvae, respectively. Gene expression on the different diets was normalized to the expression on the control diet.

(F) CG9186:GFP overexpression was either activated ubiquitously in the fat body or the oenocytes (from left to right), and the animals were grown under standard diet conditions. Subsequently, the expression of *rp49*, *CG9186*, *tobi*, and *Kr-h1* was quantified by qPCR. The expression data was normalized using *rp49* and animals lacking the overexpression.

Significance levels: *$p < 0.05$, **$p < 0.01$, and ***$p < 0.001$. Bars in (A)–(F) represent mean values of triplicate measurements. Error bars represent SEMs.

levels, which are compatible with our developmental timing and expression profiling results. Thus, our study demonstrates that CG9186 function is tied to organismic physiology regulation via interfering with JH and IIS signaling.

DISCUSSION

Based on the presence of a serine hydrolase motif and a prominent LD localization, CG9186 and its mammalian homologs were considered to play a pivotal role in lipid metabolism and to show lipolytic activity. Goo et al. (2014) reported a CE hydrolase activity for the murine CG9186 homolog LDAH, and the characterization of one LDAH knockout mouse revealed a significantly increased body weight in female mutant mice (Currall et al., 2018), which is compatible with its function as a lipase. However, these data conflict with the analysis of a second, independent LDAH knockout mouse, whose characterization did not reveal a TAG or CE metabolism-associated phenotype (Kory et al., 2017). These data also conflict with our data concerning the knock down of CG9186 transcripts by RNAi (Thiel et al., 2013) and the analysis of the null mutant presented here (Figure 1C), both of which resulted in moderately decreased TAG storage levels in adult flies and no prominent change in the TAG storage levels in whole embryos or larvae (Figures S1D and S1E). In addition, CE storage levels were not increased during the larval or adult stage (Figures S2E and S2F). Direct enzymatic activity tests for neutral lipid (TAG, DAG, MAG) and CE processing activities of CG9186 or LDAH were also negative (Kory et al., 2017; Thiel et al., 2013). Those contradictory results argue against a prominent and direct function of CG9186 in canonical storage lipid metabolism. Our finding that the overall larval fat body morphology was also unaffected by the mutation of

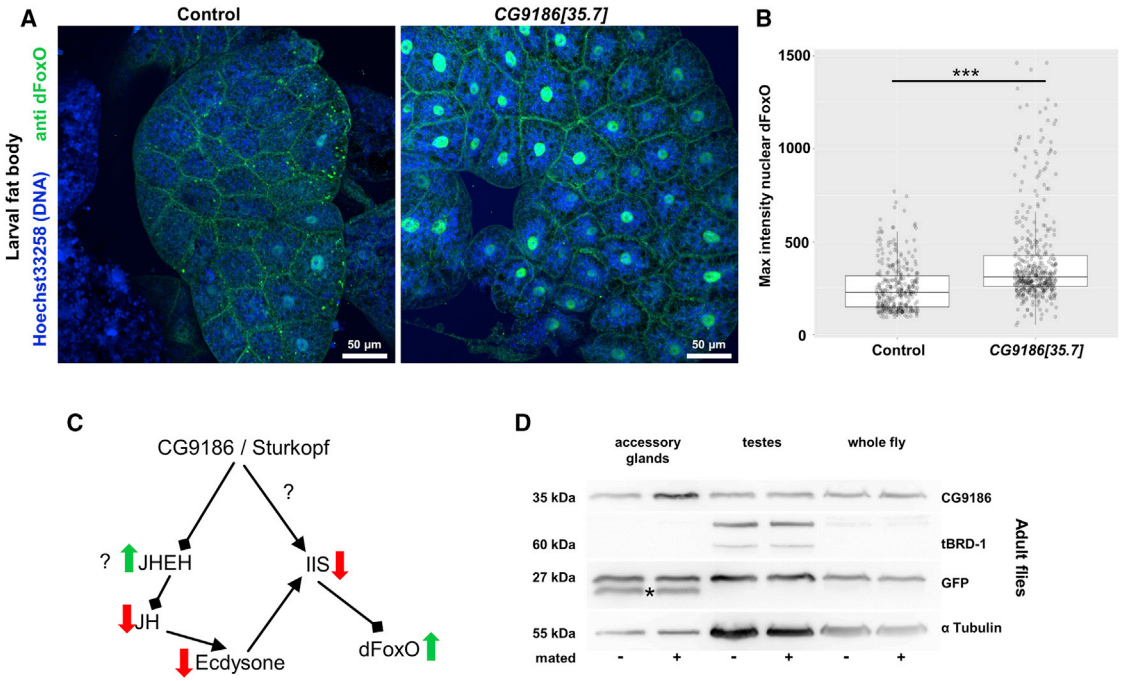

Figure 7. Altered Nuclear dFoxO Levels in Fat Bodies of CG9186 Mutant Larvae, Summarizing Model, and Expression of CG9186 in Accessory Glands

(A) Fat bodies of late wandering control or CG9186 mutant larvae were stained for DNA (Hoechst 33258; blue) or dFoxO (green).

(B) Quantification of the nuclear dFoxO levels. The boxplots represent the measurements of 315 control and 427 mutant nuclei. Representative example from three biologically independent experiments. p value obtained by a two-sample t test, with ***$p < 0.001$.

(C) Summarizing model of our findings. CG9186/sturkopf interferes with JH levels by the interaction with JHEH enzymes, and perhaps also directly affects IIS levels. JH in turn activates ecdysone, which activates IIS. IIS activity blocks dFoxO. In the CG9186/sturkopf mutant state, JHEH activity is potentially released. JH signaling is decreased, as is IIS signaling (potentially via lowered ecdysone signaling), which in turn results in increased nuclear localization, and thus activity of dFoxO. Green upward arrows mark increased activity, and red downward arrows mark decreased activity. Question marks symbolize uncertainties.

(D) Whole-fly extracts or extracts of dissected testes or accessory glands of 7-day-old virgin or mated escargot-Gal4 GFP flies (here, the promotor of the *escargot* gene drives expression of GFP in the stem-cell like secondary cells of the accessory gland) were probed with antisera specific for CG9186, the testis marker tBRD-1 (Theofel et al., 2014), anti-GFP to detect stem cells, and α-tubulin as a general loading control. Note that the GFP antibody detects a second, unspecific band in the accessory gland sample (*).

CG9186 (Figure S1F), despite its prominent expression during this stage in this tissue (Beller et al., 2006; Thiel et al., 2013), further supports this conclusion. To test for a more fine-grained impact of the CG9186 mutation on the LD lipid composition, we analyzed isolated third-instar larval fat body LDs by lipidomics. However, this level of analysis did not reveal any prominent changes (Figure S1G), which could have otherwise supported a lipid-modifying activity. Thus, why do CG9186 mutant animals store less TAG? So far, the mechanism is not completely resolved. However, our finding that IIS appears to be reduced (Figures 6A and 6C), and thus nuclear dFoxO is increased (Figures 7A and 7B), may provide an explanation. dFoxO was previously shown to affect lipid storage and fat cell mass in *Drosophila* (DiAngelo and Birnbaum, 2009) and mammals (Kousteni, 2012; Nakae et al., 2008), mostly by affecting cell size and number. Furthermore, a recent report demonstrated cooperativity of dFoxO and the JH target Kr-h1 in lipid storage regulation (Kang et al., 2017). Here, dFoxO and Kr-h1 cooperatively activate the expression of the major TAG lipase *brummer*, and thus decrease TAG storage levels (Kang et al., 2017). One report also directly linked LDAH to ATGL turnover regulation (Goo et al., 2017). Here, a lack of LDAH resulted in increased ATGL levels and therefore increased lipolysis. While we did not detect a prominently enhanced lipolysis in the starvation-refeeding experiment (Figure S2D), both processes could ultimately result in decreased TAG storage levels. Thus, the storage lipid-associated phenotypes observed by us and others could be based on the altered regulation of other factors such as ATGL/brummer instead of a direct enzymatic function of CG9186 or its mammalian relatives.

The hypothesis that the TAG-storage phenotype observed by us is based on alterations in IIS and JH signaling is further supported by the phenotypes of the CG9186 mutant flies outside the canonical lipid metabolism. Those phenotypes include the premature male lethality, the sensitivity toward oxidative stress, the altered CHC composition and desiccation protection, and the altered gene expression levels and developmental timing under nutritional stress. A possible explanation of how an ER- and LD-localized protein may result in such phenotypes can be deduced from the co-IP and split-luciferase complementation assay experiments (Figures 4A, 4B, and S5; Kolkhof et al., 2017), in which we identified an interaction between CG9186

and the JHEHs. The interaction between CG9186 and the JHEH enzymes potentially alters their amount or activity, similar to the LDAH-dependent degradation of ATGL (Goo et al., 2017). In such a model, the JHEH enzymes could show a reduced activity or enhanced degradation through CG9186 binding. A loss of CG9186 would increase JHEH abundance and/or activity, and thus a tissue-specific decrease in JH signaling due to the enhanced degradation of JH. As an alternative, CG9186 binding could enhance JHEH activity locally. On the organismic scale, however, our results demonstrate an overall reduced JH signaling activity, which would request a feedback regulation if CG9186 activates JHEH enzymes locally. Three lines of evidence support a role for CG9186 in JH signaling regulation: first, the impact of JH signaling on the CHC levels and composition was demonstrated for diverse insect species (Bontonou et al., 2015; Lengyel et al., 2007; Sledge et al., 2004), and the CG9186/sturkopf mutant does show CHC alterations (Figure 3). Second, we detected a lower expression of the JH target gene *Kruppel homolog 1* (*Kr-h1*) in CG9186 mutants (Figures 6A–6C) and higher *Kr-h1* expression levels following CG9186 overexpression (Figure 6F). Third, the CG9186/sturkopf mutant shows an altered larval developmental growth rate (Figure 6), as was previously reported for a perturbation of JH signaling (Mirth et al., 2014).

We induced altered developmental rates by changes in the food quality. The sensing of the nutritional status of an organism and the orchestration of the appropriate growth response requires the cooperative activity of multiple signaling pathways. The IIS and the target of rapamycin (TOR) signaling pathways are key to adjusting the growth rate to the environmental conditions and regulating organ and animal size (Colombani et al., 2003; Edgar, 2006; Hietakangas and Cohen, 2009; Mirth and Shingleton, 2012; Nässel and Vanden Broeck, 2016). The time point of metamorphic transition is in turn controlled by the hormones ecdysone and JH (Mirth and Shingleton, 2012). Recent evidence demonstrates that IIS and TOR signaling regulates ecdysone synthesis (Caldwell et al., 2005; Colombani et al., 2005; Layalle et al., 2008; Mirth et al., 2005), and ecdysone in turn antagonizes IIS (Colombani et al., 2005; Delanoue et al., 2010). More recently, the impact of the IIS downstream target dFoxO on the larval growth rate in response to altered JH signaling was also demonstrated (Mirth et al., 2014). The effect of JH on growth appeared to be based on an altered ecdysone synthesis in the prothoracic gland (Mirth et al., 2014). Our finding that CG9186/sturkopf apparently affects JH signaling activity is therefore in agreement with the observed changes in the developmental timing and expression of different target genes. This is particularly true for *tobi*, which is repressed by the dFoxO transcription factor (Buch et al., 2008) and whose expression in the CG9186/sturkopf mutant is extremely low. In line with these findings, nuclear dFoxO was highly increased in the CG9186/sturkopf mutant larvae (Figures 7A and 7B). A brief and simplified illustration summarizing these dependencies is shown in Figure 7C. So far, little is known concerning the differences in JH signaling activity in response to changing nutritional conditions. Our results, however, suggest that the varying activities of IIS, and perhaps also TOR signaling, may be linked to changes in JH signaling.

The signaling-associated growth phenotype of CG9186/sturkopf may guide future investigations concerning the mammalian CG9186/sturkopf homologs. So far, their function is unclear. As outlined above, the LDAH CE activity reported by Goo et al. (2014) in murine macrophages cannot yet be confirmed (Kory et al., 2017), and the CG9186 mutant did also not show a prominent cholesterol or CE storage phenotype (Figures S2E and S2F). While the murine knockout mouse also did not show obvious alterations in basal metabolic parameters (which were affected by the *Drosophila* gene mutation as, e.g., blood sugar or organismic TAG storage levels), the strength of the respective effect may depend on the diet used. The diet-dependent growth phenotype of CG9186 mutant larvae supports such a notion (Figure 5), and a second analysis of an LDAH knockout mouse revealed a moderate obesity phenotype in female mice (Currall et al., 2018). In humans, there have been multiple reports of highly significant correlations between SNPs in the CG9186 orthologous gene c2orf43 and prostate cancer (Du et al., 2016; Innocenti et al., 2011; Long et al., 2012; Takata et al., 2010; Wang et al., 2013). A recent report revealed that c2orf43 is at least 2-fold downregulated in prostate cancer samples as compared to healthy control samples (Du et al., 2016). A human patient with a heterozygous mutation resulting in lowered c2orf43 expression levels had prostate cancer and congenital hearing loss early in life (Currall et al., 2018). Further experiments using different prostate cancer cell line models and an LDAH knockout mouse resulted in strong data showing that a loss of c2orf43/LDAH results in prostate cancer initiation and progression (Currall et al., 2018). How this happens mechanistically is unknown. While JH signaling appears to be insect specific, the JHEH enzymes are homologous to the mammalian epoxide hydrolase 1 (EPHX1) enzyme (Gramates et al., 2017). EPHX1 participates in endocannabinoid signaling (Nithipatikom et al., 2014), which plays an emerging role in prostate cancer (Díaz-Laviada, 2011). Furthermore, EPHX1 detoxifies both endogenous and exogenous compounds, including procarcinogens (Václavíková et al., 2015). In combination with the existence of genetic EPHX1 variants with functional consequences, >200 association studies (http://www.cancerindex.org/geneweb/EPHX1.htm) were performed and demonstrated a strong association between EPHX1 variants and different types of cancer (Andrew et al., 2009; Goode et al., 2011; Jourenkova-Mironova et al., 2000; Sarmanová et al., 2004; Spurdle et al., 2007). Our findings may provide an entry point to investigate whether the lack of growth control, as seen in the CG9186 mutant larvae, and the impact of the loss of CG9186/sturkopf on growth-related signaling pathways are important for this process. CG9186/sturkopf is expressed in the accessory gland of flies, and its expression is upregulated upon mating (Figure 7D), which is often seen for accessory gland proteins. Only recently was the male accessory gland proposed to serve as a model to investigate certain aspects of mammalian prostate cancer (Ito et al., 2014; Wilson et al., 2017). Our study thus provides an entry point to investigate the intriguing possibility that a LD-associated protein is involved in the endocrine regulation of physiology. As the protein shuttles between the ER, where JHEHs and the microsomal EPHX1 enzymes are localized, and the LDs, the possibility arises that the transfer of CG9186/sturkopf to LDs serves a regulatory function,

as the LD localization could represent a site of sequestration. As the emergence and remobilization of LDs are linked to nutritional status, such a mechanism could also explain the diet-dependent effects observed by us.

STAR★METHODS

Detailed methods are provided in the online version of this paper and include the following:

- KEY RESOURCES TABLE
- CONTACT FOR REAGENT AND RESOURCE SHARING
- EXPERIMENTAL MODEL AND SUBJECT DETAILS
  - Fly stocks and fly husbandry
  - Tissue culture cells
- METHOD DETAILS
  - CRISPR/Cas9 mediated generation of CG9186 null mutant alleles
  - Microscopy
  - Gravimetrics
  - Lifespan Experiments
  - Fecundity Experiments
  - Desiccation Resistance
  - Measurement of Locomotor Activity
  - Larval Size Measurements
  - Starvation Resistance
  - Sensitivity Toward Oxidative Stress
  - TBA-RS Quantification
  - Protein Measurement
  - Triglyceride Measurement
  - Trehalose and Glucose Quantification (Total and Haemolymph)
  - Cholesterol and Cholesterol Ester Measurement
  - Food Intake Quantification
  - Sample Preparation for CG9186 Protein-Protein Interaction Analysis and Split Luciferase Protein Complementation Assays
  - Western Blotting
  - Liquid Chromatography Coupled Mass Spectrometric Analysis of Proteins
  - Lipidomics
  - Cuticular Hydrocarbon Analysis
  - RNA Preparation and qPCR
  - Larval Fat Body Antibody Stainings
- QUANTIFICATION AND STATISTICAL ANALYSIS
- DATA AND SOFTWARE AVAILABILITY

SUPPLEMENTAL INFORMATION

Supplemental Information can be found with this article online at https://doi.org/10.1016/j.celrep.2019.02.110.

ACKNOWLEDGMENTS

We thank Petra Kolkhof and Sandra Karpinski for excellent technical help, Kevin Kuder and Lisa Jehrke for support during the locomotor activity and CHC measurements, Simon Stockhorst for support during the early phase of the project, Thomas Klein and Clive Wilson for reagents and fly stocks, Alex Gould for the oenocyte-specific Gal4 activator fly line and the CHC analysis protocol, Pierre Leopold for the dFoxO antibody, Christina Rathke and Renate Renkawitz-Pohl for the tBRD-1 antibody, and Michael Welte for valuable comments on the manuscript. The project was funded by the Deutsche Forschungsgemeinschaft (DFG) (BE4597/2-1) and in part by the Bundesministerium für Bildung und Forschung (BMBF) (031A306), the Strategic Research Funds (F2012/297-6), and the Stiftung für Altersforschung of the University of Düsseldorf (to M.B.) and the DFG through the CRC1208 (project Z01 to K.S.).

AUTHOR CONTRIBUTIONS

M.W. and M.B. conceived and designed the experiments. M.W., F.A.S., A.G., T.M.-A., I.A., K.M.-E., A.D., T.O.E., G.P., and M.B. performed the experiments. M.W., F.A.S., A.G., T.M.-A., I.A., K.M.-E., T.O.E., G.P., K.S., and M.B. analyzed the data. M.W., G.P., and M.B. wrote the paper.

DECLARATION OF INTERESTS

The authors declare no competing interests.

Received: July 20, 2017
Revised: May 8, 2018
Accepted: February 27, 2019
Published: March 26, 2019

SUPPORTING CITATIONS

The following references appear in the Supplemental Information: Hentze et al. (2015); Jindra et al. (2015); Liu et al. (2016); Sawamura, et al. (2010).

REFERENCES

Andrew, A.S., Gui, J., Sanderson, A.C., Mason, R.A., Morlock, E.V., Schned, A.R., Kelsey, K.T., Marsit, C.J., Moore, J.H., and Karagas, M.R. (2009). Bladder cancer SNP panel predicts susceptibility and survival. Hum. Genet. *125*, 527–539.

Arcaz, A.C., Huestis, D.L., Dao, A., Yaro, A.S., Diallo, M., Andersen, J., Blomquist, G.J., and Lehmann, T. (2016). Desiccation tolerance in Anopheles coluzzii: the effects of spiracle size and cuticular hydrocarbons. J. Exp. Biol. *219*, 1675–1688.

Arrese, E.L., Saudale, F.Z., and Soulages, J.L. (2014). Lipid Droplets as Signaling Platforms Linking Metabolic and Cellular Functions. Lipid Insights *7*, 7–16.

Beller, M., Riedel, D., Jänsch, L., Dieterich, G., Wehland, J., Jäckle, H., and Kühnlein, R.P. (2006). Characterization of the Drosophila lipid droplet subproteome. Mol. Cell. Proteomics *5*, 1082–1094.

Bontonou, G., Denis, B., and Wicker-Thomas, C. (2013). Interaction between temperature and male pheromone in sexual isolation in Drosophila melanogaster. J. Evol. Biol. *26*, 2008–2020.

Bontonou, G., Shaik, H.A., Denis, B., and Wicker-Thomas, C. (2015). Acp70A regulates Drosophila pheromones through juvenile hormone induction. Insect Biochem. Mol. Biol. *56*, 36–49.

Buch, S., Melcher, C., Bauer, M., Katzenberger, J., and Pankratz, M.J. (2008). Opposing effects of dietary protein and sugar regulate a transcriptional target of Drosophila insulin-like peptide signaling. Cell Metab. *7*, 321–332.

Caldwell, P.E., Walkiewicz, M., and Stern, M. (2005). Ras activity in the Drosophila prothoracic gland regulates body size and developmental rate via ecdysone release. Curr. Biol. *15*, 1785–1795.

Carvalho, M., Sampaio, J.L., Palm, W., Brankatschk, M., Eaton, S., and Shevchenko, A. (2012). Effects of diet and development on the Drosophila lipidome. Mol. Syst. Biol. *8*, 600.

Cermelli, S., Guo, Y., Gross, S.P., and Welte, M.A. (2006). The lipid-droplet proteome reveals that droplets are a protein-storage depot. Curr. Biol. *16*, 1783–1795.

Chung, H., and Carroll, S.B. (2015). Wax, sex and the origin of species: dual roles of insect cuticular hydrocarbons in adaptation and mating. BioEssays *37*, 822–830.

Colombani, J., Raisin, S., Pantalacci, S., Radimerski, T., Montagne, J., and Léopold, P. (2003). A nutrient sensor mechanism controls Drosophila growth. Cell *114*, 739–749.

Colombani, J., Bianchini, L., Layalle, S., Pondeville, E., Dauphin-Villemant, C., Antoniewski, C., Carré, C., Noselli, S., and Léopold, P. (2005). Antagonistic actions of ecdysone and insulins determine final size in Drosophila. Science *310*, 667–670.

Currall, B.B., Chen, M., Sallari, R.C., Cotter, M., Wong, K.E., Robertson, N.G., Penney, K.L., Lunardi, A., Reschke, M., Hickox, A.E., et al. (2018). Loss of LDAH associated with prostate cancer and hearing loss. Hum. Mol. Genet. *27*, 4194–4203.

D'Ambrosio, D.N., Walewski, J.L., Clugston, R.D., Berk, P.D., Rippe, R.A., and Blaner, W.S. (2011). Distinct populations of hepatic stellate cells in the mouse liver have different capacities for retinoid and lipid storage. PLoS One *6*, e24993.

Delanoue, R., Slaidina, M., and Léopold, P. (2010). The steroid hormone ecdysone controls systemic growth by repressing dMyc function in Drosophila fat cells. Dev. Cell *18*, 1012–1021.

Dembeck, L.M., Böröczky, K., Huang, W., Schal, C., Anholt, R.R., and Mackay, T.F. (2015). Genetic architecture of natural variation in cuticular hydrocarbon composition in Drosophila melanogaster. eLife *4*, e09861.

DiAngelo, J.R., and Birnbaum, M.J. (2009). Regulation of fat cell mass by insulin in Drosophila melanogaster. Mol. Cell. Biol. *29*, 6341–6352.

Díaz-Laviada, I. (2011). The endocannabinoid system in prostate cancer. Nat. Rev. Urol. *8*, 553–561.

Ding, Y., Yang, L., Zhang, S., Wang, Y., Du, Y., Pu, J., Peng, G., Chen, Y., Zhang, H., Yu, J., et al. (2012). Identification of the major functional proteins of prokaryotic lipid droplets. J. Lipid Res. *53*, 399–411.

Djawdan, M., Chippindale, A.K., Rose, M.R., and Bradley, T.J. (1998). Metabolic reserves and evolved stress resistance in Drosophila melanogaster. Physiol. Zool. *71*, 584–594.

Du, M., Tillmans, L., Gao, J., Gao, P., Yuan, T., Dittmar, R.L., Song, W., Yang, Y., Sahr, N., Wang, T., et al. (2016). Chromatin interactions and candidate genes at ten prostate cancer risk loci. Sci. Rep. *6*, 23202.

Edgar, B.A. (2006). How flies get their size: genetics meets physiology. Nat. Rev. Genet. *7*, 907–916.

Everaerts, C., Farine, J.-P., Cobb, M., and Ferveur, J.-F. (2010). Drosophila cuticular hydrocarbons revisited: mating status alters cuticular profiles. PLoS One *5*, e9607.

Fei, W., Zhong, L., Ta, M.T., Shui, G., Wenk, M.R., and Yang, H. (2011). The size and phospholipid composition of lipid droplets can influence their proteome. Biochem. Biophys. Res. Commun. *415*, 455–462.

Fiehn, O., Kopka, J., Dörmann, P., Altmann, T., Trethewey, R.N., and Willmitzer, L. (2000). Metabolite profiling for plant functional genomics. Nat. Biotechnol. *18*, 1157–1161.

Finkel, T. (2015). The metabolic regulation of aging. Nat. Med. *21*, 1416–1423.

Folch, J., Lees, M., and Sloane Stanley, G.H. (1957). A simple method for the isolation and purification of total lipides from animal tissues. J. Biol. Chem. *226*, 497–509.

Gefen, E., Marlon, A.J., and Gibbs, A.G. (2006). Selection for desiccation resistance in adult Drosophila melanogaster affects larval development and metabolite accumulation. J. Exp. Biol. *209*, 3293–3300.

Giannakou, M.E., Goss, M., Jünger, M.A., Hafen, E., Leevers, S.J., and Partridge, L. (2004). Long-lived Drosophila with overexpressed dFOXO in adult fat body. Science *305*, 361.

Goo, Y.-H., Son, S.-H., Kreienberg, P.B., and Paul, A. (2014). Novel lipid droplet-associated serine hydrolase regulates macrophage cholesterol mobilization. Arterioscler. Thromb. Vasc. Biol. *34*, 386–396.

Goo, Y.-H.H., Son, S.-H.H., and Paul, A. (2017). Lipid Droplet-Associated Hydrolase Promotes Lipid Droplet Fusion and Enhances ATGL Degradation and Triglyceride Accumulation. Sci. Rep. *7*, 2743.

Goode, E.L., White, K.L., Vierkant, R.A., Phelan, C.M., Cunningham, J.M., Schildkraut, J.M., Berchuck, A., Larson, M.C., Fridley, B.L., Olson, J.E., et al.; Ovarian Cancer Association Consortium; Australian Ovarian Cancer Study Group (2011). Xenobiotic-Metabolizing gene polymorphisms and ovarian cancer risk. Mol. Carcinog. *50*, 397–402.

Gramates, L.S., Marygold, S.J., Santos, G.D., Urbano, J.-M.M., Antonazzo, G., Matthews, B.B., Rey, A.J., Tabone, C.J., Crosby, M.A., Emmert, D.B., et al.; the FlyBase Consortium (2017). FlyBase at 25: looking to the future. Nucleic Acids Res. *45* (*D1*), D663–D671.

Guruharsha, K.G., Rual, J.-F.F., Zhai, B., Mintseris, J., Vaidya, P., Vaidya, N., Beekman, C., Wong, C., Rhee, D.Y., Cenaj, O., et al. (2011). A protein complex network of Drosophila melanogaster. Cell *147*, 690–703.

Hartler, J., Trötzmüller, M., Chitraju, C., Spener, F., Köfeler, H.C., and Thallinger, G.G. (2011). Lipid Data Analyzer: unattended identification and quantitation of lipids in LC-MS data. Bioinformatics *27*, 572–577.

Hentze, J.L., Carlsson, M.A., Kondo, S., Nässel, D.R., and Rewitz, K.F. (2015). The Neuropeptide Allatostatin A Regulates Metabolism and Feeding Decisions in Drosophila. Sci. Rep. *5*, 11680.

Hielscher, B., Charton, L., Mettler-Altmann, T., and Linka, N. (2017). Analysis of Peroxisomal β-Oxidation During Storage Oil Mobilization in Arabidopsis thaliana Seedlings. Methods Mol. Biol. *1595*, 291–304.

Hietakangas, V., and Cohen, S.M. (2009). Regulation of tissue growth through nutrient sensing. Annu. Rev. Genet. *43*, 389–410.

Hildebrandt, A., Bickmeyer, I., and Kühnlein, R.P. (2011). Reliable Drosophila body fat quantification by a coupled colorimetric assay. PLoS One *6*, e23796.

Hodges, B.D., and Wu, C.C. (2010). Proteomic insights into an expanded cellular role for cytoplasmic lipid droplets. J. Lipid Res. *51*, 262–273.

Innocenti, F., Cooper, G.M., Stanaway, I.B., Gamazon, E.R., Smith, J.D., Mirkov, S., Ramirez, J., Liu, W., Lin, Y.S., Moloney, C., et al. (2011). Identification, replication, and functional fine-mapping of expression quantitative trait loci in primary human liver tissue. PLoS Genet. *7*, e1002078.

Ito, S., Ueda, T., Ueno, A., Nakagawa, H., Taniguchi, H., Kayukawa, N., and Miki, T. (2014). A genetic screen in Drosophila for regulators of human prostate cancer progression. Biochem. Biophys. Res. Commun. *451*, 548–555.

Jindra, M., Uhlirova, M., Charles, J.-P., Smykal, V., and Hill, R.J. (2015). Genetic Evidence for Function of the bHLH-PAS Protein Gce/Met As a Juvenile Hormone Receptor. PLoS Genet. *11*, e1005394.

Jourenkova-Mironova, N., Mitrunen, K., Bouchardy, C., Dayer, P., Benhamou, S., and Hirvonen, A. (2000). High-activity microsomal epoxide hydrolase genotypes and the risk of oral, pharynx, and larynx cancers. Cancer Res. *60*, 534–536.

Kahm, M., Hasenbrink, G., Lichtenberg-Fraté, H., Ludwig, J., and Kschischo, M. (2010). grofit: fitting biological growth curves with R. J. Stat. Softw. *33*, 1–21.

Kamimura, M., Takahashi, M., Kikuchi, K., Reza, A.M., and Kiuchi, M. (2007). Tissue-specific regulation of juvenile hormone esterase gene expression by 20-hydroxyecdysone and juvenile hormone in Bombyx mori. Arch. Insect Biochem. Physiol. *65*, 143–151.

Kamita, S.G., and Hammock, B.D. (2010). Juvenile hormone esterase: biochemistry and structure. J. Pestic. Sci. *35*, 265–274.

Kang, P., Chang, K., Liu, Y., Bouska, M., Birnbaum, A., Karashchuk, G., Thakore, R., Zheng, W., Post, S., Brent, C.S., et al. (2017). Drosophila Kruppel homolog 1 represses lipolysis through interaction with dFOXO. Sci. Rep. *7*, 16369.

Kaushik, S., Rodriguez-Navarro, J.A., Arias, E., Kiffin, R., Sahu, S., Schwartz, G.J., Cuervo, A.M., and Singh, R. (2011). Autophagy in hypothalamic AgRP neurons regulates food intake and energy balance. Cell Metab. *14*, 173–183.

Kayukawa, T., Minakuchi, C., Namiki, T., Togawa, T., Yoshiyama, M., Kamimura, M., Mita, K., Imanishi, S., Kiuchi, M., Ishikawa, Y., and Shinoda, T. (2012). Transcriptional regulation of juvenile hormone-mediated induction of Krüppel homolog 1, a repressor of insect metamorphosis. Proc. Natl. Acad. Sci. USA *109*, 11729–11734.

Kayukawa, T., Jouraku, A., Ito, Y., and Shinoda, T. (2017). Molecular mechanism underlying juvenile hormone-mediated repression of precocious larval-adult metamorphosis. Proc. Natl. Acad. Sci. USA *114*, 1057–1062.

Kelstrup, H.C., Hartfelder, K., Nascimento, F.S., and Riddiford, L.M. (2014). The role of juvenile hormone in dominance behavior, reproduction and cuticular pheromone signaling in the caste-flexible epiponine wasp, Synoeca surinama. Front. Zool. *11*, 78.

Kelstrup, H.C., Hartfelder, K., Esterhuizen, N., and Wossler, T.C. (2017). Juvenile hormone titers, ovarian status and epicuticular hydrocarbons in gynes and workers of the paper wasp Belonogaster longitarsus. J. Insect Physiol. *98*, 83–92.

Kim, J., and Neufeld, T.P. (2015). Dietary sugar promotes systemic TOR activation in Drosophila through AKH-dependent selective secretion of Dilp3. Nat. Commun. *6*, 6846.

Kimmel, A.R., and Sztalryd, C. (2016). The Perilipins: Major Cytosolic Lipid Droplet-Associated Proteins and Their Roles in Cellular Lipid Storage, Mobilization, and Systemic Homeostasis. Annu. Rev. Nutr. *36*, 471–509.

Knittelfelder, O.L., Weberhofer, B.P., Eichmann, T.O., Kohlwein, S.D., and Rechberger, G.N. (2014). A versatile ultra-high performance LC-MS method for lipid profiling. J. Chromatogr. B Analyt. Technol. Biomed. Life Sci. *951-952*, 119–128.

Kolkhof, P., Werthebach, M., van de Venn, A., Poschmann, G., Chen, L., Welte, M., Stühler, K., and Beller, M. (2017). A Luciferase-fragment Complementation Assay to Detect Lipid Droplet-associated Protein-Protein Interactions. Mol. Cell. Proteomics *16*, 329–345.

Kondo, S., and Ueda, R. (2013). Highly improved gene targeting by germline-specific Cas9 expression in Drosophila. Genetics *195*, 715–721.

Kory, N., Grond, S., Kamat, S.S., Li, Z., Krahmer, N., Chitraju, C., Zhou, P., Fröhlich, F., Semova, I., Ejsing, C., et al. (2017). Mice lacking lipid droplet-associated hydrolase, a gene linked to human prostate cancer, have normal cholesterol ester metabolism. J. Lipid Res. *58*, 226–235.

Kousteni, S. (2012). FoxO1, the transcriptional chief of staff of energy metabolism. Bone *50*, 437–443.

Layalle, S., Arquier, N., and Léopold, P. (2008). The TOR pathway couples nutrition and developmental timing in Drosophila. Dev. Cell *15*, 568–577.

Lengyel, F., Westerlund, S.A., and Kaib, M. (2007). Juvenile hormone III influences task-specific cuticular hydrocarbon profile changes in the ant Myrmicaria eumenoides. J. Chem. Ecol. *33*, 167–181.

Li, L., Zhang, H., Wang, W., Hong, Y., Wang, J., Zhang, S., Xu, S., Shu, Q., Li, J., Yang, F., et al. (2016). Comparative proteomics reveals abnormal binding of ATGL and dysferlin on lipid droplets from pressure overload-induced dysfunctional rat hearts. Sci. Rep. *6*, 19782.

Lindström, S., Schumacher, F.R., Campa, D., Albanes, D., Andriole, G., Berndt, S.I., Bueno-de-Mesquita, H.B., Chanock, S.J., Diver, W.R., Ganziano, J.M., et al. (2012). Replication of five prostate cancer loci identified in an Asian population–results from the NCI Breast and Prostate Cancer Cohort Consortium (BPC3). Cancer Epidemiol. Biomarkers Prev. *21*, 212–216.

Linford, N.J., Bilgir, C., Ro, J., and Pletcher, S.D. (2013). Measurement of lifespan in Drosophila melanogaster. J. Vis. Exp. (*71*), 50068.

Liu, Y., Liao, S., Veenstra, J.A., and Nässel, D.R. (2016). Drosophila insulin-like peptide 1 (DILP1) is transiently expressed during non-feeding stages and reproductive dormancy. Sci. Rep. *6*, 26620.

Long, Q.-Z.Z., Du, Y.-F.F., Ding, X.-Y.Y., Li, X., Song, W.-B.B., Yang, Y., Zhang, P., Zhou, J.-P.P., and Liu, X.-G.G. (2012). Replication and fine mapping for association of the C2orf43, FOXP4, GPRC6A and RFX6 genes with prostate cancer in the Chinese population. PLoS One *7*, e37866.

Lü, F.-G., Fu, K.-Y., Guo, W.-C., and Li, G.-Q. (2015). Characterization of two juvenile hormone epoxide hydrolases by RNA interference in the Colorado potato beetle. Gene *570*, 264–271.

Meunier, N., Belgacem, Y.H., and Martin, J.-R.R. (2007). Regulation of feeding behaviour and locomotor activity by takeout in Drosophila. J. Exp. Biol. *210*, 1424–1434.

Mirth, C.K., and Shingleton, A.W. (2012). Integrating body and organ size in Drosophila: recent advances and outstanding problems. Front. Endocrinol. (Lausanne) *3*, 49.

Mirth, C., Truman, J.W., and Riddiford, L.M. (2005). The role of the prothoracic gland in determining critical weight for metamorphosis in Drosophila melanogaster. Curr. Biol. *15*, 1796–1807.

Mirth, C.K., Tang, H.Y., Makohon-Moore, S.C., Salhadar, S., Gokhale, R.H., Warner, R.D., Koyama, T., Riddiford, L.M., and Shingleton, A.W. (2014). Juvenile hormone regulates body size and perturbs insulin signaling in Drosophila. Proc. Natl. Acad. Sci. USA *111*, 7018–7023.

Mitsui, T., and Riddiford, L.M. (1978). Hormonal requirements for the larval-pupal transformation of the epidermis of Manduca sexta in vitro. Dev. Biol. *62*, 193–205.

Nakae, J., Cao, Y., Oki, M., Orba, Y., Sawa, H., Kiyonari, H., Iskandar, K., Suga, K., Lombes, M., and Hayashi, Y. (2008). Forkhead transcription factor FoxO1 in adipose tissue regulates energy storage and expenditure. Diabetes *57*, 563–576.

Nässel, D.R., and Vanden Broeck, J. (2016). Insulin/IGF signaling in Drosophila and other insects: factors that regulate production, release and post-release action of the insulin-like peptides. Cell. Mol. Life Sci. *73*, 271–290.

Nithipatikom, K., Endsley, M.P., Pfeiffer, A.W., Falck, J.R., and Campbell, W.B. (2014). A novel activity of microsomal epoxide hydrolase: metabolism of the endocannabinoid 2-arachidonoylglycerol. J. Lipid Res. *55*, 2093–2102.

Ouimet, M., and Marcel, Y.L. (2012). Regulation of lipid droplet cholesterol efflux from macrophage foam cells. Arterioscler. Thromb. Vasc. Biol. *32*, 575–581.

Parkash, R., and Aggarwal, D.D. (2012). Trade-off of energy metabolites as well as body color phenotypes for starvation and desiccation resistance in montane populations of Drosophila melanogaster. Comp. Biochem. Physiol. A Mol. Integr. Physiol. *161*, 102–113.

Penney, K.L., Sinnott, J.A., Tyekucheva, S., Gerke, T., Shui, I.M., Kraft, P., Sesso, H.D., Freedman, M.L., Loda, M., Mucci, L.A., and Stampfer, M.J. (2015). Association of prostate cancer risk variants with gene expression in normal and tumor tissue. Cancer Epidemiol. Biomarkers Prev. *24*, 255–260.

Pfaffl, M.W., Horgan, G.W., and Dempfle, L. (2002). Relative expression software tool (REST) for group-wise comparison and statistical analysis of relative expression results in real-time PCR. Nucleic Acids Res. *30*, e36.

Rösch, K., Kwiatkowski, M., Hofmann, S., Schöbel, A., Grüttner, C., Wurlitzer, M., Schlüter, H., and Herker, E. (2016). Quantitative Lipid Droplet Proteome Analysis Identifies Annexin A3 as a Cofactor for HCV Particle Production. Cell Rep. *16*, 3219–3231.

Rzezniczak, T.Z., Douglas, L.A., Watterson, J.H., and Merritt, T.J. (2011). Paraquat administration in Drosophila for use in metabolic studies of oxidative stress. Anal. Biochem. *419*, 345–347.

Sarmanová, J., Sůsová, S., Gut, I., Mrhalová, M., Kodet, R., Adámek, J., Roth, Z., and Soucek, P. (2004). Breast cancer: role of polymorphisms in biotransformation enzymes. Eur. J. Hum. Genet. *12*, 848–854.

Sawamura, K., Maehara, K., Mashino, S., Kagesawa, T., Kajiwara, M., Matsuno, K., Takahashi, A., and Takano-Shimizu, T. (2010). Introgression of Drosophila simulans nuclear pore protein 160 in Drosophila melanogaster alone does not cause inviability but does cause female sterility. Genetics *186*, 669–676.

Schmidt, C., Ploier, B., Koch, B., and Daum, G. (2013). Analysis of yeast lipid droplet proteome and lipidome. Methods Cell Biol. *116*, 15–37.

Servetnick, D.A., Brasaemle, D.L., Gruia-Gray, J., Kimmel, A.R., Wolff, J., and Londos, C. (1995). Perilipins are associated with cholesteryl ester droplets in steroidogenic adrenal cortical and Leydig cells. J. Biol. Chem. *270*, 16970–16973.

Shui, I.M., Lindström, S., Kibel, A.S., Berndt, S.I., Campa, D., Gerke, T., Penney, K.L., Albanes, D., Berg, C., Bueno-de-Mesquita, H.B., et al. (2014). Prostate cancer (PCa) risk variants and risk of fatal PCa in the National Cancer Institute Breast and Prostate Cancer Cohort Consortium. Eur. Urol. *65*, 1069–1075.

Sledge, M.F., Trinca, I., Massolo, A., Boscaro, F., and Turillazzi, S. (2004). Variation in cuticular hydrocarbon signatures, hormonal correlates and establishment of reproductive dominance in a polistine wasp. J. Insect Physiol. *50*, 73–83.

Spurdle, A.B., Chang, J.-H., Byrnes, G.B., Chen, X., Dite, G.S., McCredie, M.R., Giles, G.G., Southey, M.C., Chenevix-Trench, G., and Hopper, J.L. (2007). A systematic approach to analysing gene-gene interactions: polymorphisms at the microsomal epoxide hydrolase EPHX and glutathione S-transferase GSTM1, GSTT1, and GSTP1 loci and breast cancer risk. Cancer Epidemiol. Biomarkers Prev. *16*, 769–774.

Takata, R., Akamatsu, S., Kubo, M., Takahashi, A., Hosono, N., Kawaguchi, T., Tsunoda, T., Inazawa, J., Kamatani, N., Ogawa, O., et al. (2010). Genome-wide association study identifies five new susceptibility loci for prostate cancer in the Japanese population. Nat. Genet. *42*, 751–754.

Tennessen, J.M., Barry, W.E., Cox, J., and Thummel, C.S. (2014). Methods for studying metabolism in Drosophila. Methods *68*, 105–115.

Theofel, I., Bartkuhn, M., Hundertmark, T., Boettger, T., Gärtner, S.M., Leser, K., Awe, S., Schipper, M., Renkawitz-Pohl, R., and Rathke, C. (2014). tBRD-1 selectively controls gene activity in the Drosophila testis and interacts with two new members of the bromodomain and extra-terminal (BET) family. PLoS One *9*, e108267.

Thiam, A., and Beller, M. (2017). The why, when and how of lipid droplet diversity. J. Cell. Sci. *130*, 315–324.

Thiel, K., Heier, C., Haberl, V., Thul, P.J., Oberer, M., Lass, A., Jäckle, H., and Beller, M. (2013). The evolutionarily conserved protein CG9186 is associated with lipid droplets, required for their positioning and for fat storage. J. Cell Sci. *126*, 2198–2212.

Tusher, V.G., Tibshirani, R., and Chu, G. (2001). Significance analysis of microarrays applied to the ionizing radiation response. Proc. Natl. Acad. Sci. USA *98*, 5116–5121.

Tusun, A., Li, M., Liang, X., Yang, T., Yang, B., and Wang, G. (2017). Juvenile Hormone Epoxide Hydrolase: a Promising Target for Hemipteran Pest Management. Sci. Rep. *7*, 789.

Václavíková, R., Hughes, D.J., and Souček, P. (2015). Microsomal epoxide hydrolase 1 (EPHX1): Gene, structure, function, and role in human disease. Gene *571*, 1–8.

Vermunt, A.M., Vermeesch, A.M., and de Kort, C.A. (1997). Purification and characterization of juvenile hormone esterase from hemolymph of the Colorado potato beetle. Arch. Insect Biochem. Physiol. *35*, 261–277.

Vrablik, T.L., Petyuk, V.A., Larson, E.M., Smith, R.D., and Watts, J.L. (2015). Lipidomic and proteomic analysis of Caenorhabditis elegans lipid droplets and identification of ACS-4 as a lipid droplet-associated protein. Biochim. Biophys. Acta *1851*, 1337–1345.

Wang, N.-N.N., Xu, Y., Yang, K., Wei, D., Zhang, Y.-G.G., Liu, M., Shi, X.-H.H., Liang, S.-Y.Y., Sun, L., Zhu, X.-Q.Q., et al. (2013). Susceptibility loci associations with prostate cancer risk in northern Chinese men. Asian Pac. J. Cancer Prev. *14*, 3075–3078.

Welte, M.A. (2015). Expanding roles for lipid droplets. Curr. Biol. *25*, R470–R481.

Wilson, C., Leiblich, A., Goberdhan, D.C.I., and Hamdy, F. (2017). The Drosophila Accessory Gland as a Model for Prostate Cancer and Other Pathologies. Curr. Top. Dev. Biol. *121*, 339–375.

Wojtasek, H., and Prestwich, G.D. (1996). An insect juvenile hormone-specific epoxide hydrolase is related to vertebrate microsomal epoxide hydrolases. Biochem. Biophys. Res. Commun. *220*, 323–329.

Yoshida, M., Matsuda, H., Kubo, H., and Nishimura, T. (2016). Molecular characterization of Tps1 and Treh genes in Drosophila and their role in body water homeostasis. Sci. Rep. *6*, 30582.

Yue, S., Li, J., Lee, S.-Y., Lee, H.J., Shao, T., Song, B., Cheng, L., Masterson, T.A., Liu, X., Ratliff, T.L., and Cheng, J.X. (2014). Cholesteryl ester accumulation induced by PTEN loss and PI3K/AKT activation underlies human prostate cancer aggressiveness. Cell Metab. *19*, 393–406.

Zhang, H., Wang, Y., Li, J., Yu, J., Pu, J., Li, L., Zhang, H., Zhang, S., Peng, G., Yang, F., and Liu, P. (2011). Proteome of skeletal muscle lipid droplet reveals association with mitochondria and apolipoprotein a-I. J. Proteome Res. *10*, 4757–4768.

Zimmermann, R., Strauss, J.G., Haemmerle, G., Schoiswohl, G., Birner-Gruenberger, R., Riederer, M., Lass, A., Neuberger, G., Eisenhaber, F., Hermetter, A., and Zechner, R. (2004). Fat mobilization in adipose tissue is promoted by adipose triglyceride lipase. Science *306*, 1383–1386.

STAR★METHODS

KEY RESOURCES TABLE

REAGENT or RESOURCE	SOURCE	IDENTIFIER
Antibodies		
Rabbit anti-dFoxO	Delanoue et al., 2010	NA
Rat anti-CG9186	Thiel et al., 2013	NA
Mouse anti-alpha Tubulin	Sigma-Aldrich	Cat# T5168; RRID: AB_477579
Rabbit anti-GFP	Torrey Pines Labs	Cat# TP401; RRID: AB_2313770
Rabbit anti-tBRD-1	Theofel et al., 2014	NA
GFP trap A beads	Chromotek	Cat# gta-20; RRID: AB_2631357
Chemicals, Peptides, and Recombinant Proteins		
BODIPY 493/503 lipid stain	Thermo Fisher Scientific	Cat# D3922
Hoechst 33258	Sigma-Aldrich	Cat# B2883
Critical Commercial Assays		
Pierce BCA Protein Assay Kit	Thermo Fisher Scientific	Cat# 23225
Infinity Triglycerides reagent	Thermo Fisher Scientific	Cat# 981786
Glucose GO Assay Kit	Sigma-Aldrich	Cat# GAGO20
Amplex Red Cholesterol Assay Kit	Thermo Fisher Scientific	Cat# A12216
RNeasy Mini Kit	QIAGEN	Cat# 74104
QuantiTect Reverse Transcription kit	QIAGEN	Cat# 205310
GoScript Reverse Transcription kit	Promega	Cat# A5000
GoTaq qPCR Master Mix	Promega	Cat# A6001
Deposited Data		
Protein-protein interaction mass spectrometric raw data and searches	This study	PRIDE repository @ https://www.ebi.ac.uk/pride/archive/ ID: PXD006457
Experimental Models: Cell Lines		
D. melanogaster: Cell line Kc167: Kc167-DRSC	Laboratory of Norbert Perrimon	FlyBase: FBtc0000001
Drosophila Kc167 expressing GFP	Kolkhof et al., 2017	NA
Drosophila Kc167 expressing CG9186:GFP	Kolkhof et al., 2017	NA
Experimental Models: Organisms/Strains		
w1118;;	This study	MBD470
w1118;; $CG9186^{35.1}$/ $CG9186^{35.1}$	This study	MBD478
w1118;; $CG9186^{35.2}$/ $CG9186^{35.2}$	This study	MBD471
w1118;; $CG9186^{35.6}$/ $CG9186^{35.6}$	This study	MBD472
w1118;; $CG9186^{35.7}$/ $CG9186^{35.7}$	This study	MBD473
w^{-};If/CyO^{wglacZ};MKRS(Sb)/TM6b(Hu,Tb,e)	Laboratory of Thomas Klein	NA
Cas9 source: yw;attP40{nos-Cas9}/CyO	BestGene / Kondo and Ueda, 2013	MBD474
w^{-};;MKRS(Sb)/TM6b(Hu,Tb,e)	Laboratory of Thomas Klein	MBD475
w^{-};;+/TM3(Sb)	This study	NA
w;esg-GAL4 tub-GAL80ts UAS-GFPnls/CyO;UAS-flp act > CD2 > GAL4/TM6	Laboratory of Clive Wilson	MBD476
UAS CG9186:eGFP	Thiel et al., 2013	MBD73
w*; P{w[+mW.hs] = GawB}FB+SNS	Beller et al., 2006	MBD59
wh; PromE(200)-Gal4	Laboratory of Alex Gould	MBD525
w*; P{w[+mC] = tubP-GAL4}LL7/CyO	Laboratory of Herbert Jäckle	MBD75
Oligonucleotides		
Please see Table S1		

(*Continued on next page*)

Continued

REAGENT or RESOURCE	SOURCE	IDENTIFIER
Recombinant DNA		
CG9186 CRISPR targeting (sgRNA in ORF): TCTCTTACGATTACAGCCATAGG	This study	pBFv-U6.2_DC26 / MBD 602
CG9186 CRISPR targeting (sgRNA in UTR): TTTATCAGAGCTATCAACCCTGG	This study	pBFv-U6.2_MB2 / MBD735
GCN4 leucine zipper gluc(1) c-term	Kolkhof et al., 2017	MBD396
GCN4 leucine zipper gluc(2) c-term	Kolkhof et al., 2017	MBD397
CG9186 gluc(1) c-term	Kolkhof et al., 2017	MBD453
JHEH1 gluc(2) c-term	This study	MBD879
JHEH2 gluc(2) c-term	This study	MBD881
JHEH3 gluc(2) c-term	This study	MBD883
Software and Algorithms		
R programming language		https://www.r-project.org/
Grofit package	Kahm et al., 2010	https://www.rdocumentation.org/packages/grofit/versions/1.1.1-1
Survminer package		https://rpkgs.datanovia.com/survminer/index.html
Zen Light software version 2.4	Zeiss	N/A
REST software	Pfaffl et al., 2002	http://rest.gene-quantification.info/
MassHunter Qual software	Agilent	N/A
MassLynx version 4.1	Waters	N/A
MaxQuant version 1.5.5.1	MPI for Biochemistry, Planegg, Germany	https://www.biochem.mpg.de/5111795/maxquant

CONTACT FOR REAGENT AND RESOURCE SHARING

Further information and requests for resources and reagents should be directed to and will be fulfilled by the Lead Contact, Mathias Beller (mathias.beller@hhu.de).

EXPERIMENTAL MODEL AND SUBJECT DETAILS

Fly stocks and fly husbandry

If not stated otherwise, *D. melanogaster* stocks were kept at 25°C with a 12 h light/dark cycle. All fly stocks used are mentioned in the Key Resources Table. For the sex, age and/or stage of the animals used in the given experiment please refer to the corresponding text or figure legend. In the course of the experiments we used two different control diets with the following recipes:

Control diet 1: (for 100 mL) 0.624 g agar, 8 g polenta, 1 g soy flour, 1.8 g dry yeast, 2.2 g treacle, 8 g malt extract, 1.5 mL nipagin (10% in 70% ethanol) and 0.63 mL propionic acid.
Control diet 2: (for 100 mL) 0.5 g agar, 7.1 g polenta, 0.95 g soy flour, 1.68 g dry yeast, 4 g treacle, 4.5 g malt extract,1.5 mL nipagin (10% in 70% ethanol), 0.45 mL propionic acid.

For stock maintenance and the lifespan experiments we used control diet 2. Control diet 1 served as the basis for the food supplementation experiments as outlined below:

Low-sugar diet: (for 100 mL) 1 g agar, 8 g dry yeast, 2 g bacto-yeast-extract, 2 g bacto-peptone, 5.13 g sucrose, 2 mM $MgSO_4$, 3.4 mM $CaCl_2$, 1 mL nipagin (10% in 70% ethanol), 0.6 mL propionic acid.
Low-yeast diet: The low-yeast diet is based on standard diet 1 but contains instead of 1.8 g yeast only 0.18 g.
High fat diet: The high fat diet is also based on standard diet 1 but additionally contains 10% coconut oil, which replaces the equivalent volume of water.

Tissue culture cells

We used *Drosophila* Kc167 cells which are embryonic female hemocytes. The cells were obtained from the Harvard RNAi Screening Center (Laboratory of Norbert Perrimon). Cells were grown in Schneider's medium (PAN Biotech) supplemented with 10% FCS (PAN Biotech) and Penicillin/Streptomycin according to general culturing protocols.

METHOD DETAILS

CRISPR/Cas9 mediated generation of CG9186 null mutant alleles

CG9186 null alleles were generated according to Kondo and Ueda (2013). Potential gRNA sites within the *CG9186* gene were identified using the *DRSC Find CRISPR (version 2)* tool (https://www.flyrnai.org/crispr2/). To induce a > 1000 bp deletion which can easily be detected via simple PCR, two gRNA-coding sequences were chosen, one located in the CDS at position 3L:1311958..1311980 (+ strand) (TCTCTTACGATTACAGCCATAGG), the other in the UTR at position 3L:1313094..1313116 (- strand) (TTTATCAGAGCTATCAACCCTGG). Oligonucleotides coding for these two sequences were obtained from the Harvard CRISPr Resource pre-cloned into the pBFv-U6.2 vector (Kondo and Ueda, 2013). The combined plasmids were injected into > 200 embryos of a *yw;nos-Cas9(II-attp40)* strain (genotype: *yw;attP40{nos-Cas9}/CyO*) by BestGene Inc. (Chino Hills, CA, USA). Following the injection, a total of 36 animals hatched and were single crossed (cross #1 to #36) with a multibalancer strain (w^{-}*;If/CyO*$^{wg\text{-}lacZ}$*; MKRS(Sb)/TM6b(Hu,Tb,e)*). From every successful single cross, six to seven hatching flies were again single crossed with multibalancer flies (e.g., #1.1 to 1.7) and the progeny was screened for successful mutagenesis with PCR. For the PCR, primers flanking the predicted lesion were used. Of 36 injected animals, two individuals showed a mosaic germline and produced mutant progeny (#6 and #35). Mutant flies were backcrossed with a w^{-}*;;MKRS(Sb)/TM6b(Hu,Tb,e)* strain in order to remove all markers from the second chromosome and then again crossed with w^{-}*;;+/TM3(Sb)* flies to swop balancers. To generate a genetically matched control strain, uninjected *yw;nos-Cas9(II-attp40)* flies were crossed in exactly the same way. Of the two different sets of mutants, only the progeny of fly #35 was homozygous viable and was therefore used in all experiments. To verify that the mutant flies actually lack CG9186 protein, western blot experiments with a CG9186 specific antibody (Thiel et al., 2013) were performed. The lesions in two of the generated null-alleles (#35.2 and #35.7) were further characterized by sequencing using primers listed in Table S1.

Microscopy

Organs were dissected in ice cold PBS and fixed for 20 min in 5% paraformaldehyde. Subsequently, LDs and nuclei were stained with 1:2000 BODIPY 493/503 (Thermo Fisher Scientific, Waltham, USA) and 1:500 Hoechst33258 (Sigma Aldrich, St. Louis, USA) in PBS, respectively. Organs were embedded in Mowiol and imaged using a Zeiss LSM780 confocal microscope.

Gravimetrics

To investigate body mass and water content, 30 animals were anaesthetized with CO_2, transferred to a pre-weighed 2 mL tube and weighed on an analytical scale. Afterward, the tube was snap-frozen in liquid nitrogen, then opened and the dead flies were dried in a drying chamber for at least 24 hours at 60°C, followed by another weighing step.

Lifespan Experiments

Lifespan experiments were conducted according to Linford et al. (2013). About 300 flies per genotype were anesthetized and transferred to a cage with an attached apple agar plate with fresh yeast paste. After 24 h at 25°C, the plate was discarded and a new plate with fresh yeast paste was attached. Following another 20 h, embryos were carefully removed from the plate using 10 mL of PBT (PBS with 0.1% Tween20) and a brush, and they were transferred to a 15 mL tube. After the embryos settled, the supernatant was removed, and the embryos were washed with PBT until the supernatant became clear. In one final washing step, PBS was used. After the embryos settled again, 33 μL of the embryos were transferred to a fly vial containing control diet food by the use of a wide bore pipette tip. The animals were allowed to develop at 25°C with a 12 h light / dark cycle. One day after the flies started to hatch all animals were discarded. After another day, the flies were transferred to standard fly vials in groups of about 60-70 animals. The flies were allowed to mate for two days and then females and males were separated and transferred to new vials in groups of exactly 30 animals. For the measurement of lifespan, flies from at least four vials (120 animals per sex and genotype) were transferred to new vials every two to three days and monitored for survival. If not stated otherwise, flies for all stress experiments and metabolic assays were seven days old and derived from the procedure described for the lifespan experiments.

Fecundity Experiments

Two five to seven day old virgin females are combined with one virgin male fly of the same age per vial. Every day, the flies are transferred at the same time point to a fresh vial and the embryos are counted. After three to four days the parental flies are discarded. In order to monitor the hatchability rate, the number of pupae in each vial are counted and related to the number of eggs laid. For each condition, we analyzed at least ten vials per experiment.

Desiccation Resistance

In order to investigate the flies' sensitivity toward desiccation, 30 flies (seven days old) were transferred to an empty vial and kept at 25°C without any source of food or water and monitored for survival every one to twelve hours. For each sex, genotype or experimental condition at least three vials were tested.

Measurement of Locomotor Activity

Locomotor activity was recorded on a TriKinetics Dam2 Activity Monitoring System using a standard 10% sucrose in agar medium as food source, or without any nutritional or water source (desiccation assays). Recordings were carried out in a temperature controlled incubator with a 12 hours dark/light cycle. Data analysis was performed with custom scripts which are provided in the form of a webtool under the following URL: https://mathias-beller.shinyapps.io/trikinetics_activitymonitor/.

Larval Size Measurements

To analyze larval development, 50-60 adult flies (seven days old, developed as described for lifespan experiments) were transferred to fresh vials with either standard medium or special medium, e.g., low-yeast or low-sugar. On the next day, flies were again transferred to new vials. After 16 hours, adult flies were discarded, and the vials were kept at 25°C (12 h light / dark cycle). For each genotype and medium, at least three vials were used as technical replicates. Development was monitored in two ways: 1) Vials were monitored and the occurrence of pupae was counted at least two to three times per day giving a growth curve for each vial. 2) At different time points, 20-30 larvae were removed from the medium, washed with ice cold PBS and pictures of the larvae were taken with a Zeiss SteREO Discovery.V8 microscope and an ICc 5 AxioCam. The imaged larvae were encircled and measured with the Zeiss ZEN Blue (2012) Software, which results in mm^2 surface area values.

Starvation Resistance

To monitor for survival under total absence of nutrients, 30 flies (seven days old) were transferred to a vial containing 0.5% agarose in water and monitored for survival every four to twelve hours while being kept at 25°C. For each sex and genotype, at least four vials were used.

Sensitivity Toward Oxidative Stress

Oxidative stress was induced with Paraquat (Methylviologen). A total of 30 flies (seven days old) were transferred in a vial containing a 2x7 cm piece of whatman paper soaked with 800 μL of 20 mM Paraquat (in 5% sucrose in water). The vials were kept at 25°C. For each sex and genotype, at least four vials were used. As a control, 30 additional flies were kept in a vial with 5% sucrose only. Dead flies were counted every four to twelve hours.

TBA-RS Quantification

For the measurement of thiobarbituric acid reactive substances (TBA-RS), 20 flies were homogenized in a 1.5 mL reaction tube with an electrical pellet pestle and 200 μL of ice cold PBS. 125 μL of this homogenate was mixed with 187.5 μL phosphoric acid (0.44 M) and 62.5 μL thiobarbituric acid (TBA, 0.6% in H_2O), and incubated for 40 min at 100°C. The remaining homogenate was used for protein normalization (see metabolic measurements). The amount of TBA-RS was subsequently measured fluorometrically by a BioTek Synergy Mx plate reader (BioTek Germany, Bad Friedrichshall) with 530 nm excitation and 550 nm emission wavelengths.

Protein Measurement

Protein was determined using the Pierce BCA Protein Assay Kit following the manufacturer's instructions. Protein values were used to normalize the measurements of the other metabolites, e.g., triglyceride and cholesterol.

Triglyceride Measurement

Triglyceride quantification was performed as described in Hildebrandt et al. (2011). In brief, eight adult flies or five L3 larvae were transferred to a 2 mL screw cap tube and homogenized in 0.05% Tween20 in H_2O (males and larvae in 500 μL, females in 1000 μL) with a BIO101/Savant FastPrep FP120 Cell disruptor (Qbiogene, Illkirch, France). The homogenate was heat inactivated for 5 min at 70°C and centrifuged at 5000 rpm for 5 min. The supernatant was transferred to a new tube and again centrifuged at 14800 rpm for 15 minutes. 50 μL of this sample was transferred to two wells of a clear 96 well plate. One well was used for protein, the other for triglyceride measurement. For triglycerides, 200 μL of Infinity Triglycerides reagent (Thermo Fisher Scientific, Waltham, USA) was added to each well and after 30 min of incubation at 37°C absorbance at 510 nm was measured using a Synergy Mx plate reader (BioTek Germany, Bad Friedrichshall).

Trehalose and Glucose Quantification (Total and Haemolymph)

With minor alterations, trehalose levels of whole flies were measured according to Tennessen et al. (2014) with the use of the Glucose (GO) Assay Kit (Sigma Aldrich, St. Louis, USA). Eight adult flies were homogenized in 300 μL of ice cold trehalase buffer (5 mM Tris pH 6.6, 137 mM NaCl, 2.7 mM KCl) with a BIO101/Savant FastPrep FP120 Cell disruptor (Qbiogene, Illkirch, France) followed by heat inactivation of the homogenate for 10 min at 70°C. After centrifugation at full speed, 30 μL of the supernatant was transferred to two

1.5 mL tubes. To digest trehalose to free glucose, 30 μL of trehalase buffer containing porcine trehalase enzyme was added to one of the tubes. For the measurement of free glucose only, the second sample was diluted with 30 μL of trehalase buffer without any additional enzymes. For the quantification, a dilution series of glucose and trehalose standards were prepared. After incubation for 24 h at 37°C, 30 μL of each sample as well as the standards were transferred to a clear 96 well plate and mixed with 100 μL glucose reagent. After incubation for 1 h at 37°C, the reaction was stopped by adding 100 μL of 12 N H_2SO_4 and absorbance of the samples was measured at 540 nm using a Synergy Mx plate reader (BioTek Germany, Bad Friedrichshall). Trehalose content was calculated by subtracting free glucose values from the samples which were incubated with trehalase enzyme. Values were normalized to total protein content measured by a standard BCA assay.

For the measurement of haemolymph trehalose and glucose, 30 animals were anaesthetized, pricked into the thorax with an ultramicro needle (tungsten, rod diameter 0.12 mm), and transferred to a 0.5 mL tube with a small hole in the bottom. The 0.5 mL tube was quickly inserted into a 1.5 mL tube containing 50 μL of ice cold trehalase buffer and centrifuged for 5 min at 6000 rpm in a prechilled centrifuge. The sample was immediately snap frozen in liquid nitrogen, and the next sample was prepared. After heat inactivation (10 min at 70°C) and centrifugation of the samples, 2 × 15 μL of the sample were added to 2 × 45 μL trehalase buffer (measurement of glucose and protein) and another 15 μL were added to 45 μL of trehalase buffer containing porcine trehalase. Protein was measured immediately, whereas glucose and trehalose samples were incubated and measured as described above.

Cholesterol and Cholesterol Ester Measurement

With a few alterations, quantification of free cholesterol and cholesterol ester levels was carried out following the protocol by Tennessen et al. (2014) using the Amplex Red Cholesterol Assay Kit (Thermo Fisher Scientific, Waltham, USA). A total of 20 flies (seven days old) were homogenized in 500 μL 0.05% Tween20 in water using a BIO101/Savant FastPrep FP120 Cell disruptor (Qbiogene, Illkirch, France), and the homogenate was heat inactivated for 5 min at 70°C. 400 μL of the sample was transferred to a 1.5 mL tube; the rest was centrifuged, and the supernatant was used for protein measurement. To extract all lipids, 900 μL of a chloroform methanol mixture (2:1) was added to the 400 μL fly homogenate and mixed thoroughly. Lipids were extracted for 30 minutes under constant shaking. After centrifugation, the lower lipid containing phase was transferred quantitatively to a 2 mL screw cap tube and the solvent was removed under a constant nitrogen stream. Dried lipids were resolubilized in 500 μL of 1X Amplex Red reaction buffer. 100 μL of sample was transferred to two 1.5 mL tubes. To digest all cholesterol esters and measure total cholesterol, 0.4 units of cholesterol esterase was added to one of the tubes. No enzyme was added to the other tube, leaving it for the measurement of only free cholesterol. Both sets of tubes were incubated at 37°C for 3 hours. Afterward, 25 μL of sample and 25 μL of the Amplex Red Cholesterol Assay kit (Thermo Scientific, Dreieich, Germany) were added to solid, black 96 well plates and mixed with 90 μL of the reaction mix. The assay was detected fluorometrically (excitation at 530 nm, and emission at 550 nm) and quantification was based on a cholesterol standard curve.

Food Intake Quantification

One day prior to the experiment (in the afternoon), groups of 20 age matched flies (females and males separated) were transferred to vials with standard or starving medium (0.5% agarose in water, as a positive control). On the next day, animals were transferred (without anaesthetization) onto standard medium containing 200 μg/mL fluorescein. After exactly 30 min at 25°C, flies were killed by snap freezing and then washed twice with PBS to remove all traces of food. Animals were then homogenized in 300 μL 10 mM TRIS pH 7.4 and centrifuged at full speed. 100 μL of the supernatant were transferred to a black 96 well plate and fluorescence (ex 475 −490 nm, em 510 - 520 nm) was measured with a Synergy Mx plate reader (BioTek Germany, Bad Friedrichshall).

Sample Preparation for CG9186 Protein-Protein Interaction Analysis and Split Luciferase Protein Complementation Assays

CG9186:GFP co-IPs in the presence or absence of OA and using GFP as a negative control as well as the subsequent split luciferase complementation assay interaction tests were performed as described in Kolkhof et al. (2017).

Western Blotting

SDS-PAGE and western blotting were carried out according to standard procedures as reported previously (Thiel et al., 2013). We used the following antibodies: rat anti CG9186 (Thiel et al., 2013): 1:3000; mouse anti alpha-Tubulin (Sigma Aldrich, St. Louis, USA): 1:3000, rabbit anti-GFP (Torrey Pines Biolabs, Secaucus, USA): 1:2000, rabbit anti tBRD-1 (Theofel et al., 2014; kind gift from C. Rathke and R. Renkawitz-Pohl): 1:1000. All peroxidase conjugated secondary antibodies were ordered from Pierce (Thermo Scientific, Dreieich, Germany).

Liquid Chromatography Coupled Mass Spectrometric Analysis of Proteins

Proteins from anti GFP-immunoprecipitations (9186 GFP, GFP, 9186 GFP + oleate, GFP + oleate, each n = 5) were prepared for mass spectrometric analysis essentially as already described (Kolkhof et al., 2017). Briefly, samples were shortly separated in a polyacrylamide gel, after silver staining protein containing bands were cut out, destained, washed and proteins reduced with dithiothreitol, alkylated with chloroacetamide, digested with trypsin and after peptide extraction finally resuspended in 0.1% trifluoroacetic acid.

Subsequently, peptides were separated on an Ultimate 3000 RSLCnano liquid chromatography system (Thermo Scientific, Dreieich, Germany) on 25 cm long columns essentially as described earlier (Kolkhof et al., 2017) using a 1 h gradient separation.

The liquid chromatography system was coupled online to a mass spectrometer via a nano electrospray ionization source and the sample injected by distal coated Silica Tip emitters (New Objective, Woburn, MA, USA).

Immunoprecipitation samples were analyzed on an Orbitrap Elite (Thermo Scientific, Bremen, Germany) mass spectrometer, operated in data dependent positive mode using a spray voltage of 1.4 kV and capillary temperature of 275°C. Precursor scans were carried out in the orbitrap analyzer with a resolution of 60,000 (at 400 m/z) over a 350-1700 m/z mass range using a maximum fill time of 200 ms and a target value for the automatic gain control of 3,000,000. Subsequently, the top ten most intensive > 1 fold charged precursor ions were fragmented using collision induced dissociation and analyzed over an available mass range from 200 to 2,000 m/z at a resolution of 5,400 (at 400 m/z) with a maximal fill time of 10 ms and an automatic gain control target value of 30,000 in the linear ion trap part of the instrument. Already fragmented ions were excluded from further analysis for the next 15 s.

Data analysis was carried out within the MaxQuant 1.5.5.1 environment (MPI for Biochemistry, Planegg, Germany) using standard parameters if not otherwise stated. Searches were carried out against the UP000000803 *Drosophila* proteome downloaded from UniprotKB on 10th October 2016 supplemented by an entry for GFP (P42212) for the searches of the immunoprecipitation samples. Tryptic cleavage specificity was considered as well as carbamidomethyl on cysteines as fixed and methionine and N-terminal acetylation (and ubiquitinylation - glygly – for the immunoprecipitation samples) as variable modifications. Allowed mass tolerances for peptides were 20 ppm for the initial search and 4.5 ppm after recalibration. For fragment spectra the mass tolerances were 20 ppm for spectra recorded in the Orbitrap and 0.5 Da for spectra recorded in the linear ion trap part of the instrument. Peptides and proteins were accepted at a false positive rate of 1% and only proteins considered for which at least two different peptides were identified. The ''match between runs'' option was enabled as well as label free quantification.

The data of the immunoprecipitation samples was analyzed independently for the samples with oleate and the samples without oleate treatment. Only proteins were considered showing at least four valid values in one group, missing values were filled in with random values from a normal distribution (width: 0.3 standard deviations and a downshift of 1.8 standard deviations).

Student's t test were calculated on log2 transformed values using the significance analysis of microarrays method (Tusher et al., 2001) using an S_0 of 0.1 and reporting of values at a false discovery rate of 5%.

Mass spectrometry data were submitted to ProteomeXchange via the PRIDE database (PXD006457).

Lipidomics

For the lipidomics analysis, larval lipid droplets were purified by ultracentrifugation as described previously (Beller et al., 2006). Despite of the absence of a clear-cut lipid storage (CE or TAG) phenotype during the 3rd instar larval stage (Figures S1E and S2E), we used larval LDs on the basis of the following rationale: First, CG9186 is prominently expressed in the fat bodies of 3rd instar larvae (Thiel et al., 2013). Thus, the possibility to detect a phenotype was reasonably high. One could argue that a purification from adults would have been better based on the TAG and CE phenotypes detected by us. However, LDs from different tissues show enrichment for certain lipid classes such as TAGs in most lipid storing tissues (Carvalho et al., 2012) – including the fly fat body -, CE in prostate cancer cells and macrophages (Ouimet and Marcel, 2012; Yue et al., 2014), or retinol esters in stellate cells (D'Ambrosio et al., 2011). A pan-LD preparation from a mixture of tissues thus might camouflage more subtle lipid phenotypes. Further, the purification of adult *Drosophila* LDs failed so far and getting tissue-specific LDs appears even more challenging. Thus, we decided to investigate larval fat body LDs.

For the LD purification, we dissected for each genotype 30 fat bodies from 3rd instar larvae in black dishes with forceps and collected them in 100 μL Fat Body Buffer (FBB) in a 1.5 mL reaction tube. The samples were stored at −80°C until use. Before cell fractionation the fat bodies were thawed in additional 900 μL FBB and cells were ruptured with ultrasound. Afterward a sucrose gradient for each sample was built. A 10 mL 0.54 M sucrose solution containing the fat body sample formed the bottom layer. Then 3 mL of a 0.27 M and 0.135 M sucrose solution were added and 3 mL FBB constituted the top layer. The samples were ultra-centrifuged at 28,000 rpm at 4°C for 1:30 hours with a slow break. Subsequently, 800 μL of the top layer were taken off. The remaining gradient was carefully removed to isolate the microsomal pellet. Both, the lipid droplet fraction and the microsomal pellet were stored at −80°C until further use.

Total lipids were extracted twice according to Folch et al. (1957) using chloroform/methanol/water (2/1/0.6, v/v/v) containing 500 pmol butylated hydroxytoluene, 1% acetic acid, and 100 pmol of internal standards (ISTD, 17:0-17:0 PC, 17:0-17:0 PE, 17:0-17:0-17:0 TAG, 17:0 LPC, Avanti Polar Lipids) per sample. Extraction was performed under constant shaking for 60 min at room temperature (RT). After centrifugation at 1,000 x *g* for 15 min at RT the lower organic phase was collected. 2.5 mL chloroform were added to the remaining aqueous phase and the second extraction was performed as described above. Combined organic phases of the double-extraction were dried under a stream of nitrogen and resolved in 150 μL 2-propanol/chloroform/methanol (7/2/1, v/v/v) for UPLC-qTOF analysis. Chromatographic separation was modified after (Knittelfelder et al., 2014) using an AQUITY-UPLC system (Waters Corporation), equipped with an ACQUITY BEH C18 column (2.1x50 mm, 1.7 μm; Waters Corporation). A SYNAPTG1 qTOF HD mass spectrometer (Waters Corporation) equipped with an ESI source was used for detection. Data acquisition was done by the MassLynx 4.1 software (Waters Corporation) and lipid classes were analyzed with the ''Lipid Data Analyzer 1.6.2'' software (Hartler et al., 2011). Data were normalized for recovery and extraction- and ionization efficacy using ISTDs. All samples were analyzed in triplicates.

Cuticular Hydrocarbon Analysis

Hydrocarbons were washed off from five flies with 50 μL hexane (containing 0.1 mM octadecane 628 as an internal standard) by shaking for 1 min according to Dembeck et al. (2015). One μL of each hydrocarbon sample was directly applied to gas-chromatographic coupled to time-of-flight mass spectrometric analysis. For this purpose, a 7200 GC-qTOF (Agilent, U.S.A.) was used and run as described in Hielscher et al. (2017). Compounds were (i) extracted from chromatograms by deconvolution and (ii) quantified using the MassHunter Qual software (Agilent, U.S.A.). For compound identification, the National Institute of Standards and Technology (NIST) and Fiehn libraries (Fiehn et al., 2000) were searched for the resulting spectra within the MassHunter Qual software environment. The peak area of each compound was (iv) normalized to the peak area of the internal standard and used for statistical analyses in Microsoft Excel. All samples were analyzed in quadruplicates.

RNA Preparation and qPCR

For gene expression analyses, we isolated total RNA from whole larvae five days after egg laying or from migrating 3rd instar larvae. For the larval RNA extraction, we used five larvae (standard diets or low-sugar diet as well as overexpressing larvae) or 20 larvae (low-yeast diet) and the RNeasy Mini Kit following the manufacturer's instructions and a motorized pistil for homogenization in RLT buffer including DTT.

For the cDNA synthesis, we used 1 μg of total RNA per sample and either the QIAGEN QuantiTect Reverse Transcription Kit (QIAGEN, Hilden, Germany) or the GoScript Reverese Transcriptase kit (Promega, Madison, Wisconsin, USA) according to the manufacturer's instructions. The qPCR was performed using the GoTaq qPCR Master Mix (Promega, Madison, Wisconsin, USA) according to the manufacturer's instructions and a Bio-Rad thermal cycler. Data analysis was done using the REST software (Pfaffl el al., 2002) with standard settings.

Larval Fat Body Antibody Stainings

Wandering 3rd instar *Drosophila* larvae from control or *CG9186[35.7]* mutant animals were opened in PBS on ice using forceps and fixed in 4% paraformaldehyde for 20 min. Subsequently, the specimen were permeabilized using 0.3% Triton X-100 in PBS for 20 min, followed by a rebuffering and washing in BBT (Borate buffered saline (BBS), 0.1% bovine serum albumin (BSA), 0.1% Tween20) for three times. The larvae were then incubated with BBT including 2% goat serum for 30 minutes. The anti dFoxO antibody (kind gift from Dr. Pierre Leopold; dilution 1:500) was then added in BBT and incubated over night at 4°C. After multiple additional washes with BBT, the specimen were incubated for 30 min in BBT containing 2% goat serum, followed by incubation with the 1:500 diluted Alexa488 coupled secondary antibody in BBT for 2 hours. Afterward, the larvae were again washed with BBT and finally with PBS including 0.1% Tween-20 and Hoechst33258 (1μg / mL) for 20 min. Finally, the fat bodies were dissected and afterward embedded in Mowiol with two antifades (propyl-gallate and -Triethylenediamine (DABCO)). The fat bodies were imaged using a Zeiss LSM710 with a 20 x air objective. We used the same intensity settings throughout each experiment and adjusted the settings to the brightest signal. Subsequently, we recorded Z-stacks and analyzed the maximum intensity projections using the Zen Light software (version 2.4). In brief, we marked all Hoechst positive nuclei by equally sized circles and measured the green signal (coming from the dFoxO staining) in these areas. We then plotted all data in boxplots and used an unpaired two sample t test to test for significant differences.

QUANTIFICATION AND STATISTICAL ANALYSIS

Standard unpaired two-sample t tests were performed with Excel (version 2016) or the R programming language. For multiple sample comparisons, we performed a one-way ANOVA with a Tukey Post hoc test using R. Survival curves were plotted with the survminer package for the R statistical language, which was also used to perform a log-rank test for significance. Growth curves were plotted using the grofit package (Kahm et al., 2010) for R and tested for statistical significant differences using the statmod R package and a permutation test with 10,000 permutations and a Benjamini-Hochberg FDR p value correction. The identified CG9186/sturkopf interaction partners were analyzed using custom R scripts and Bioconductor packages.

DATA AND SOFTWARE AVAILABILITY

The co-IP proteomics dataset is available at the PRIDE repository accessible at https://www.ebi.ac.uk/pride/archive/ at PRIDE: PXD006457.